C O M M O N S D E E D

저작자표시-비영리-변경금지 **2.0** 대한민국

이용자는 아래의 조건을 따르는 경우에 한하여 자유롭게

- 이 저작물을 복제, 배포, 전송, 전시, 공연 및 방송할 수 있습니다.

다음과 같은 조건을 따라야 합니다:

저작자표시. 귀하는 원저작자를 표시하여야 합니다.

비영리. 귀하는 이 저작물을 영리 목적으로 이용할 수 없습니다.

변경금지. 귀하는 이 저작물을 개작, 변형 또는 가공할 수 없습니다.

- 귀하는, 이 저작물의 재이용이나 배포의 경우, 이 저작물에 적용된 이용허락조건을 명확하게 나타내어야 합니다.
- 저작권자로부터 별도의 허가를 받으면 이러한 조건들은 적용되지 않습니다.

저작권법에 따른 이용자의 권리는 위의 내용에 의하여 영향을 받지 않습니다.

이것은 이용허락규약(Legal Code)을 이해하기 쉽게 요약한 것입니다.

Disclaimer

공학박사 학위논문

Temporalis Muscle Activity Detection through Mechanically Amplified Force Measurement on Glasses

안경에서 기계적으로 증폭된 힘 측정을 통한 측두근 활동의 감지

2017년 8월

서울대학교 대학원

기계항공공학부

정 정 만

Temporalis Muscle Activity Detection through Mechanically Amplified Force Measurement on Glasses

안경에서 기계적으로 증폭된 힘 측정을 통한

측두근 활동의 감지

지도 교수 이 건 우

이 논문을 공학박사 학위논문으로 제출함

2017년 4월

서울대학교 대학원

기계항공공학부

정 정 만

정정만의 공학박사 학위논문을 인준함

2017년 6월

위 원 장 안 성 훈 (인)

부위원장 이 건 우 (인)

위 원 방 현 우 (인)

위 원 조 규 진 (인)

위 원 이 윤 구 (인)

Abstract

Recently, the form of a pair of glasses is broadly utilized as a wearable device that provides the virtual and augmented reality in addition to its natural functionality as a visual aid. These approaches, however, have lacked the use of its inherent kinematic structure, which is composed of both the temple and the hinge. When we equip the glasses, the force is concentrated at the hinge, which connects the head piece and the temple, from the law of the lever. In addition, since the temple passes through a temporalis muscle, chewing and wink activity, anatomically activated by the contraction and relaxation of the temporalis muscle, can be detected from the mechanically amplified force measurement at the hinge.

This study presents a new and effective method for automatic and objective measurement of the temporalis muscle activity through the natural-born lever mechanism of the glasses. From the implementation of the load cell-integrated wireless circuit module inserted into the both hinges of a 3D printed glasses frame, we developed the system that responds to the temporalis muscle activity persistently regardless of various form factor different from each person. This offers the potential to improve previous studies by avoiding the morphological, behavioral, and environmental constraints of using skin-attached, proximity, and sound sensors. In this study, we collected data featured as sedentary rest, chewing, walking, chewing while walking, talking and wink from 10-subject user study. The collected data were transferred to a series of 84-dimentional feature vectors, each of which was composed of the statistical features of both temporal and spectral domain. These feature vectors, then, were used to define a classifier model implemented by the support vector machine (SVM) algorithm. The model classified the featured activities (chewing, wink, and physical activity) as the average F_1 score of 93.7%.

This study provides a novel approach on the monitoring of ingestive behavior (MIB) in a non-intrusive and un-obtrusive manner. It supplies the possibility to apply the MIB into daily life by distinguishing the food intake from the other physical activities such as walking, talking, and wink with higher accuracy and wearability. Furthermore, through applying this approach to a sensor-integrated hair band, it can be potentially used for the medical monitoring of the sleep bruxism or temporomandibular dysfunction.

Keywords: Glasses, law of the lever, wearable device, monitoring of ingestive behavior (MIB), pattern recognition, support vector machine (SVM)

Student Number: 2011-20752

Contents

List of Figures

List of Tables

Chapter 1.

Introduction

1.1. Motivation

"Give me a place to stand on, and I can move the earth."

– *Archimedes, AD 340*

1.1.1. Law of the Lever

This research starts from an Archimedes' famous quote. He said that he could move the earth using a lever of sufficient length. Although this statement requires several mechanical assumptions and is physically impossible to do so in human performance, it emphasizes the mechanically simple but also effective *law of the lever*. He proved it using geometric reasoning [1].

The *lever* is the beam that pivots at a fixed *hinge*, or *fulcrum*, from the effects of input and output forces. The input and output forces are generally referred to as *effort* and *load*, respectively. In the ideal condition of no energy dissipation or storage, such as no friction at the hinge or bending of the lever, the power that enters the lever must be equal to the power that comes out from the lever. From this basis, the *moment*, or *torque, equilibrium* of the lever system can be computed as

$$\mathrm{Torque} = \mathrm{Effort} \cdot \mathrm{L_{Effort}} = \mathrm{Load} \cdot \mathrm{L_{Load}} \tag{1.1}$$

where Effort is the input force, Load is the resistant force, $\mathrm{L_{Effort}}$ is the perpendicular distance from hinge to the effort, and $\mathrm{L_{Load}}$ is the perpendicular distance from the hinge to load. This equation is known as the law of the lever.

The *mechanical advantage*, MA, of the lever is the ratio of Load to Effort, which is

$$\mathrm{MA} = \frac{\mathrm{Load}}{\mathrm{Effort}} = \frac{\mathrm{L_{Load}}}{\mathrm{L_{Effort}}}. \tag{1.2}$$

This equation shows that the mechanical advantage can be represented by geometric relationship of the hinge, load, and effort. This relationship is valid when assuming no losses and stores of energy due to friction, elasticity, etc. In the case of the lever, the effect of mechanical advantage is also referred to as *leverage*.

The levers are classified into three classes by the relative positions of the fulcrum, effort and load:

Class 1: the fulcrum is in the middle ($\mathrm{MA} > 0$).

Class 2: the load is in the middle ($\mathrm{MA} > 1$).

Class 3: the effort is in the middle ($0 < \mathrm{MA} < 1$).

Generally, the classes 1 and 2 are utilized as amplifying the force, because there is a gain of the force at the point of the load, whereas the class 3 is utilized as a precise operation because of a gain of the distance at the point of the load.

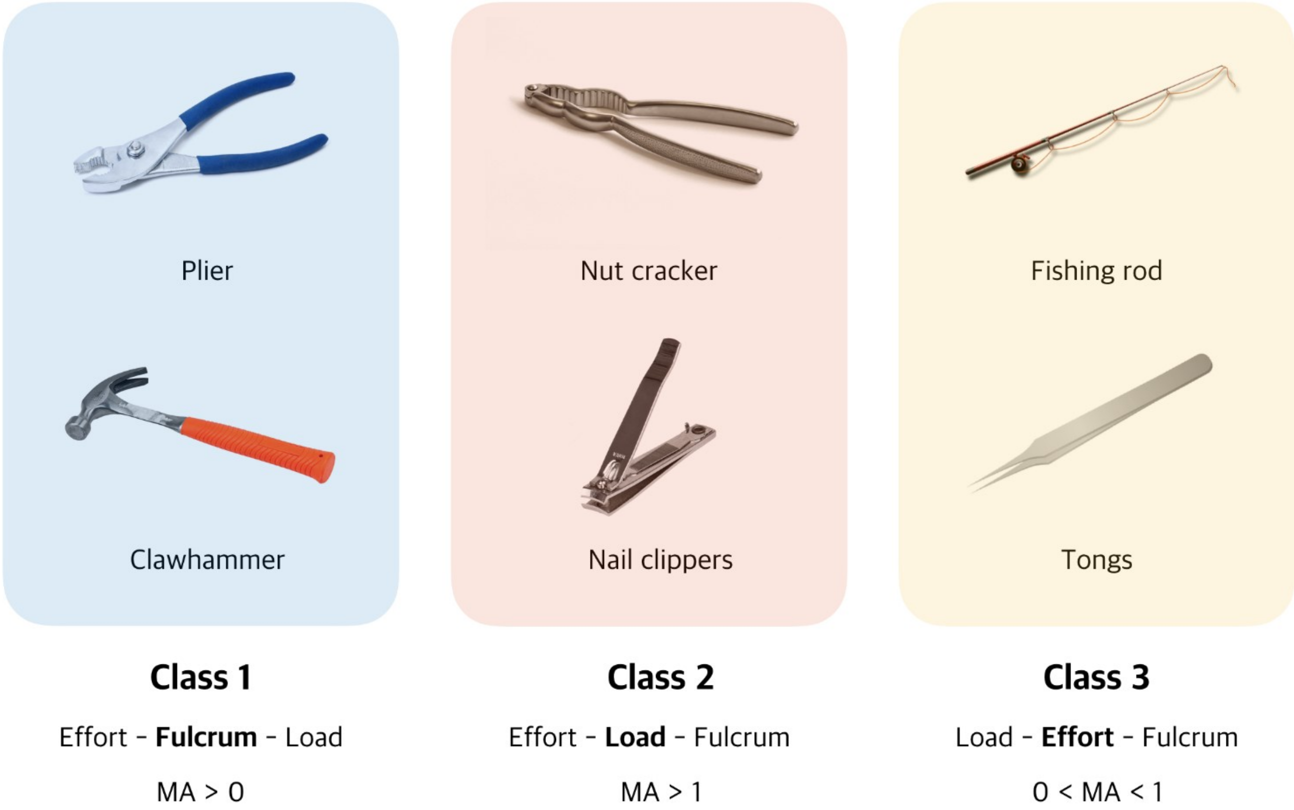

Figure 1.1 The lever mechanism in mechanical devices (a) Class 1. (b) Class 2. (c) Class 3.

1.1.2. Lever Mechanism in Human Body

The human body also utilizes the mechanical advantage from the law of the lever through musculoskeletal system. The joint between the head and the first cervical vertebra is an example of the class 1 lever. The head (load) is rotated around the cervical vertebra (hinge) by the muscle activity (effort) located in the posterior neck. Another example of the class 2 lever is when lifting of the heel from the lower leg. The body weight (load) is sustained by the Achilles tendon (effort) connected to the calf muscles around the toes (hinge). This utilizes the gain of the force. In the case of class 3 lever, an example can be found in human’s arm. From the contraction and relaxation of the biceps muscle (effort), the forearm (load) can be rotate around the elbow joint (hinge). This allows the precise operation of the hand.

1.1.3. Mechanical Advantage in Auditory Ossicle

There is only one sensory organ that utilizes the mechanical advantage in our body. Each sensory organ, such as visual, auditory, olfactory, taste, or tactile organs, receives chemical molecules, sound vibration, photons, or physical pressure, then generate chemical and electrical signals transferred to the nervous system. Among them, the auditory organ uses physical force amplification through the leverage, and force concentration to amplify the weak sound vibration. The vibration of air is amplified by the lever mechanism through the auditory ossicle, and the transmitted force is concentrated on the small stapes footplate area, compared with the large eardrum area (see Figure 1.2).

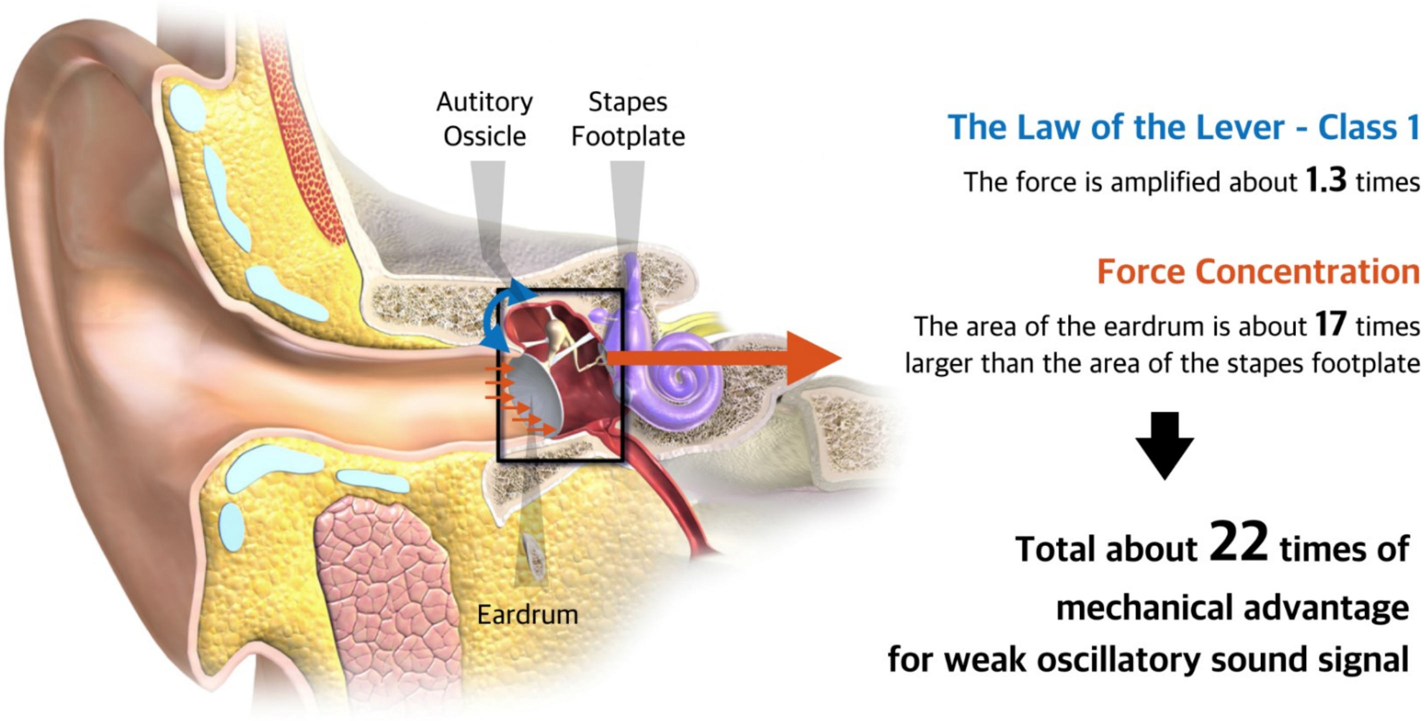

Figure 1.2 Mechanical advantage in auditory ossicle.

1.1.4. Mechanical Advantage in Glasses

If we closely look at the glasses, there is a natural−born lever mechanism from the combination of the temple (effort), hinge (fulcrum), and head piece (load). The exerted force on the temple is amplified at the hinge contacting to the head piece by the law of the lever. This lever is class 2, as the point of the load is in the middle of the effect and fulcrum. In this case, the mechanical advantage is greater than 1, which results in the force amplification as the ratio of the distance from the hinge joint to the representative point where the temple contacts with the skin of the temple to the distance from the hinge joint to the support plate of the head piece. Also, the force concentration occurs at the support plate, as the area which the force exerted is different (see Fig. 1.3).

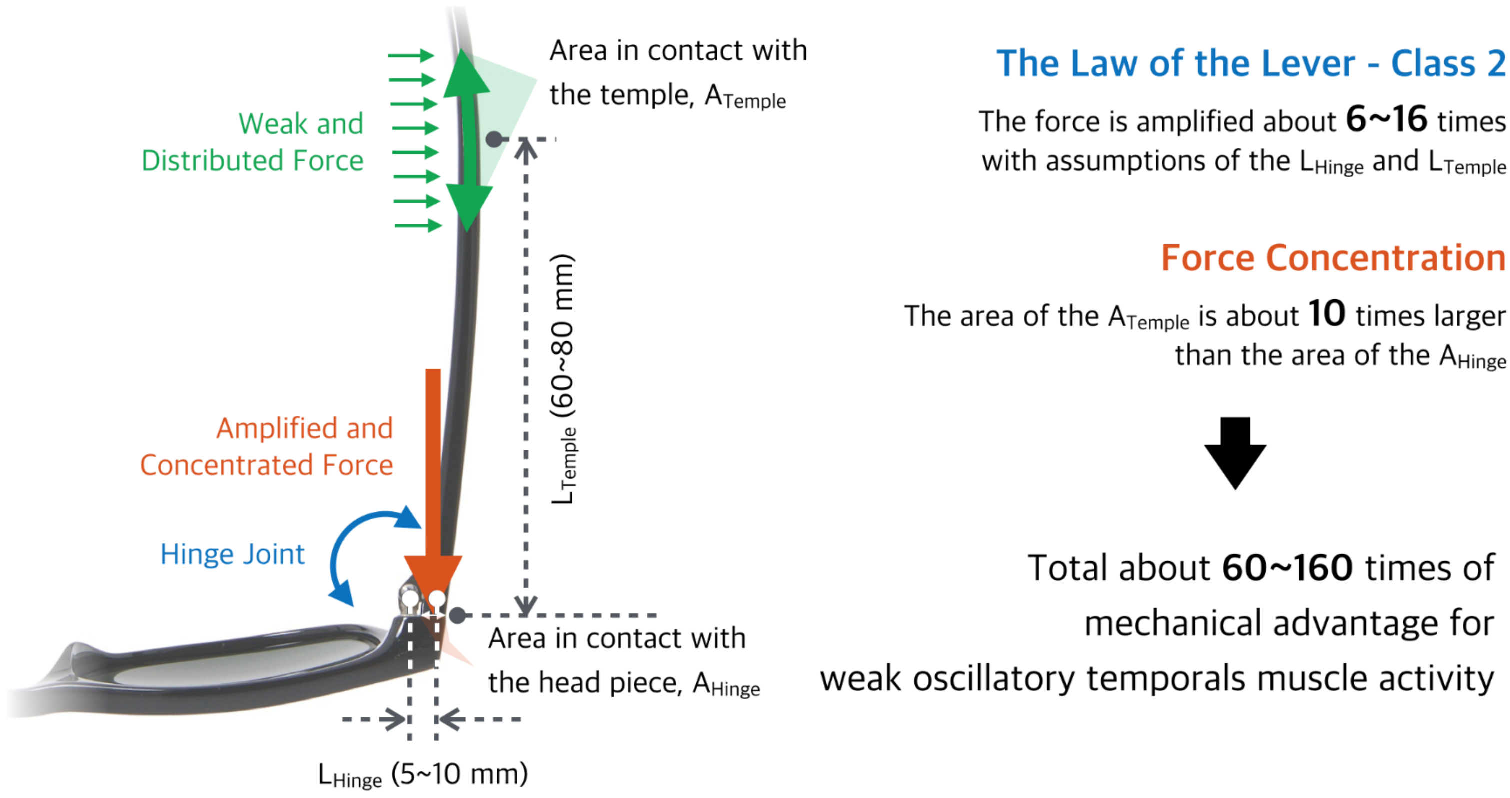

Figure 1.3 Mechanical advantage in a pair of glasses.

1.2. Background

1.2.1. Biological Information from Temporalis Muscle

This study was motivated by two ideas: (i) measurement of temporalis muscle activity due to its role as a masticatory muscle during ingestive behavior; and (ii) the natural lever mechanism of a pair of glasses, which pass through the temporalis epidermis when equipped. To explain the first idea, contraction and relaxation of the temporalis muscle result in elevation, retraction, and side-to-side grinding movements of the mandible, or lower jawbone, during the mastication cycle [2, 3]. This muscle activity results in approximate 1.2 mm changes of the muscle thickness, with a lower deviation compared with that of the masseter and sternocleidomastoid muscles for adults without temporomandibular disorder [4]. Based on this background, this study utilized oscillatory patterns of the thickness of the temporalis muscle for the monitoring of ingestive behavior (MIB). Here, we focused on the second idea and employed glasses that are fastened by friction due to a compressive force at the contact area between the temples of the glasses and the temporalis epidermis on both sides of the head. In order words, we can monitor the temporalis muscle activity by measuring the force exerted onto the temple areas of the glasses.

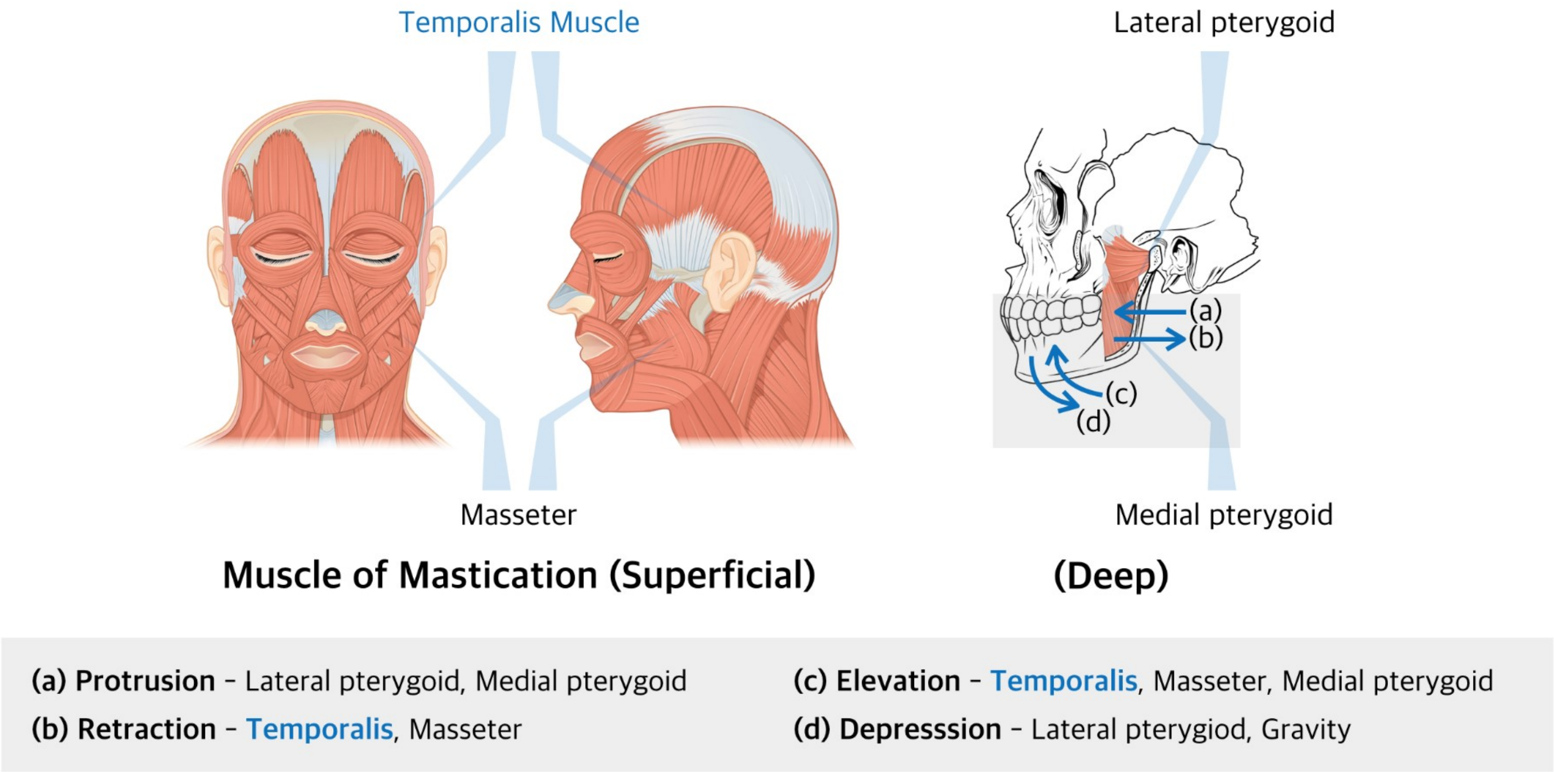

Figure 1.4 Masticatory muscles

1.2.2. Detection of Temporalis Muscle Activity

The force signal exerted on the temple, mentioned in chapter 1.2.1, has several weaknesses; (a) it is too weak to be detected directly from the contact area, (b) it is distributed over the contact area, (c) both location and form factors of the contact area differ from individual to individual, and (d) direct contact with the epidermis exposes the sensor to possible damage from perspiration and rubbing. To resolve these problems, we proposed the use of a mechanical advantage created by the natural lever mechanism of the glasses. By measuring the force on the hinge, where the temple contacts the headpiece, it becomes much easier to detect the temporalis muscle activity during ingestive behavior. This solution provides the following advantages: (a) the force is amplified by the laws of a lever, (b) the force is concentrated on the small contact area between the temple and the headpiece, (c) the uniform form factor accommodates for variety in individuals, and (d) the sensor avoids damage from direct contact with the epidermis. The graphical description of these features and advantages is illustrated in Fig. 1.6.

Recently, there has been more practical approaches to recognize chewing events with utilizing the temporalis muscle activity and a glassed-type wearable device [5, 6]. Farooq and Sazonov [7] attached a piezoelectric sensor onto temporalis epidermis to monitor chewing cycles and collected data through a Bluetooth module embedded in a pair of glasses. So, they could monitor the eating behavior even in walking condition. Zhang, Bernhart, and Amft [8] used electromyography (EMG) electrodes in a pair of 3D-printed glasses. They designed the suitable placements and the type of the EMG electrodes within the glasses. However, they had common limitations that the sensor could easily be damaged or influenced by the perspiration or hairs between the skin and the sensor. Our approaches effectively solved this problem by taking advantage of kinematics of the glasses itself. Furthermore, utilizing the two sensors on both sides could differentiate left-and-right chewing and wink events.

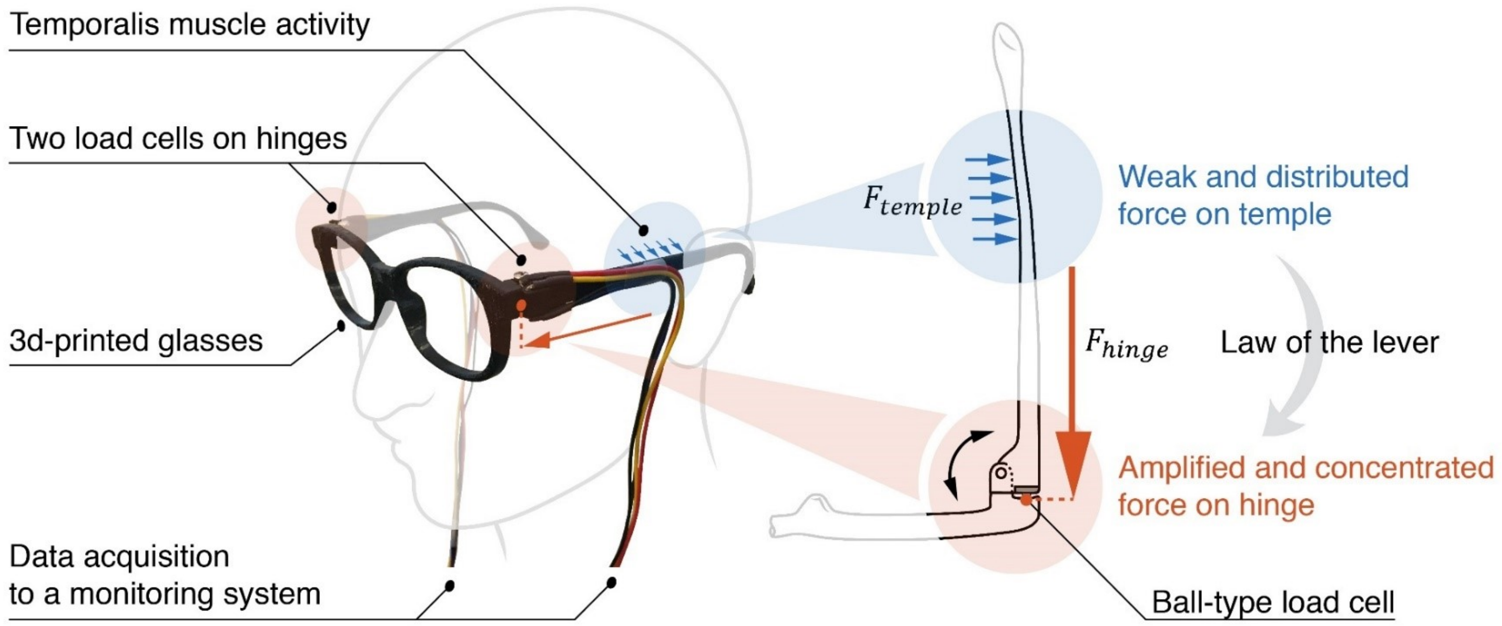

Figure 1.5 Schematic diagram of GlasSense

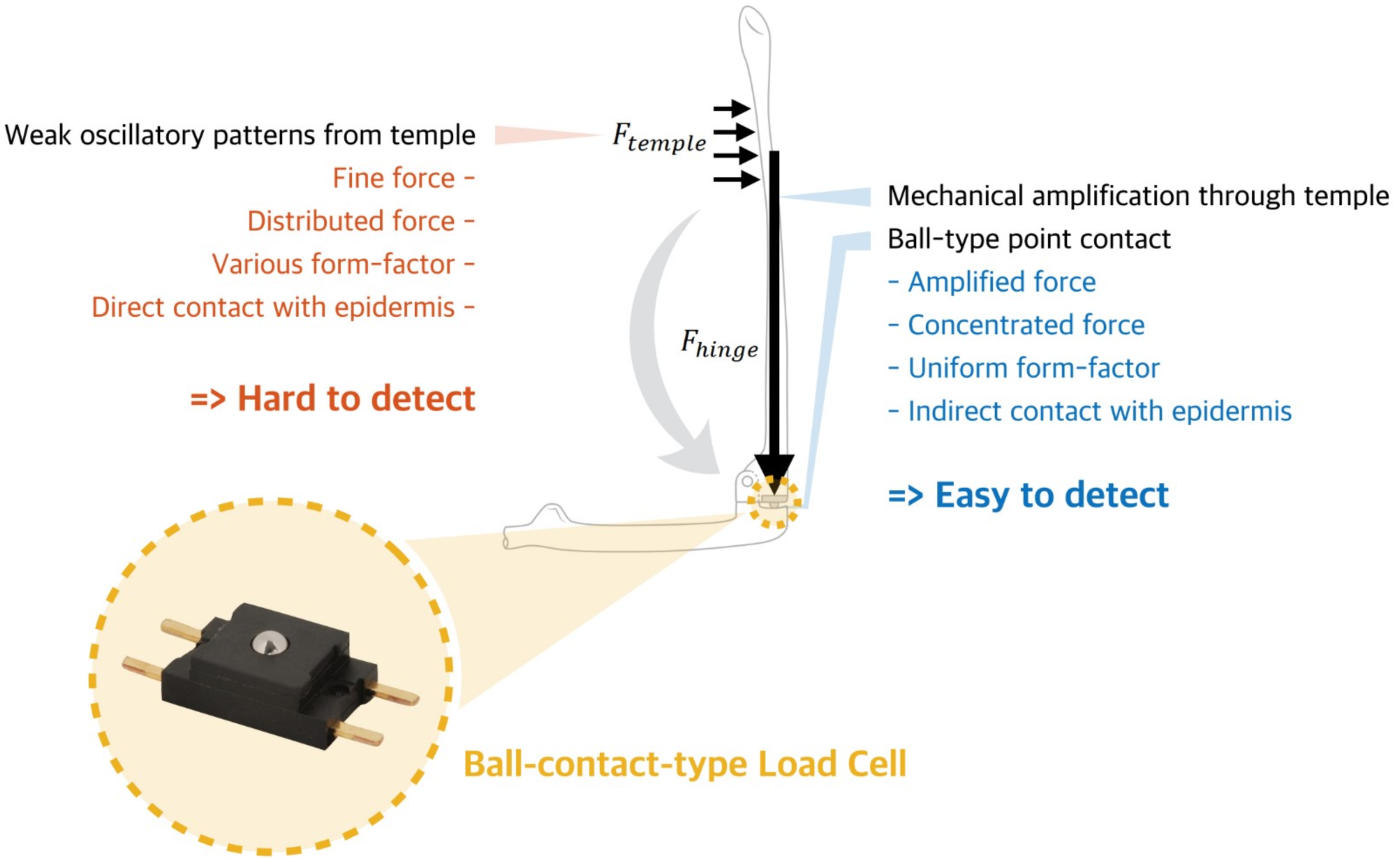

Figure 1.6 Advantage of the solution

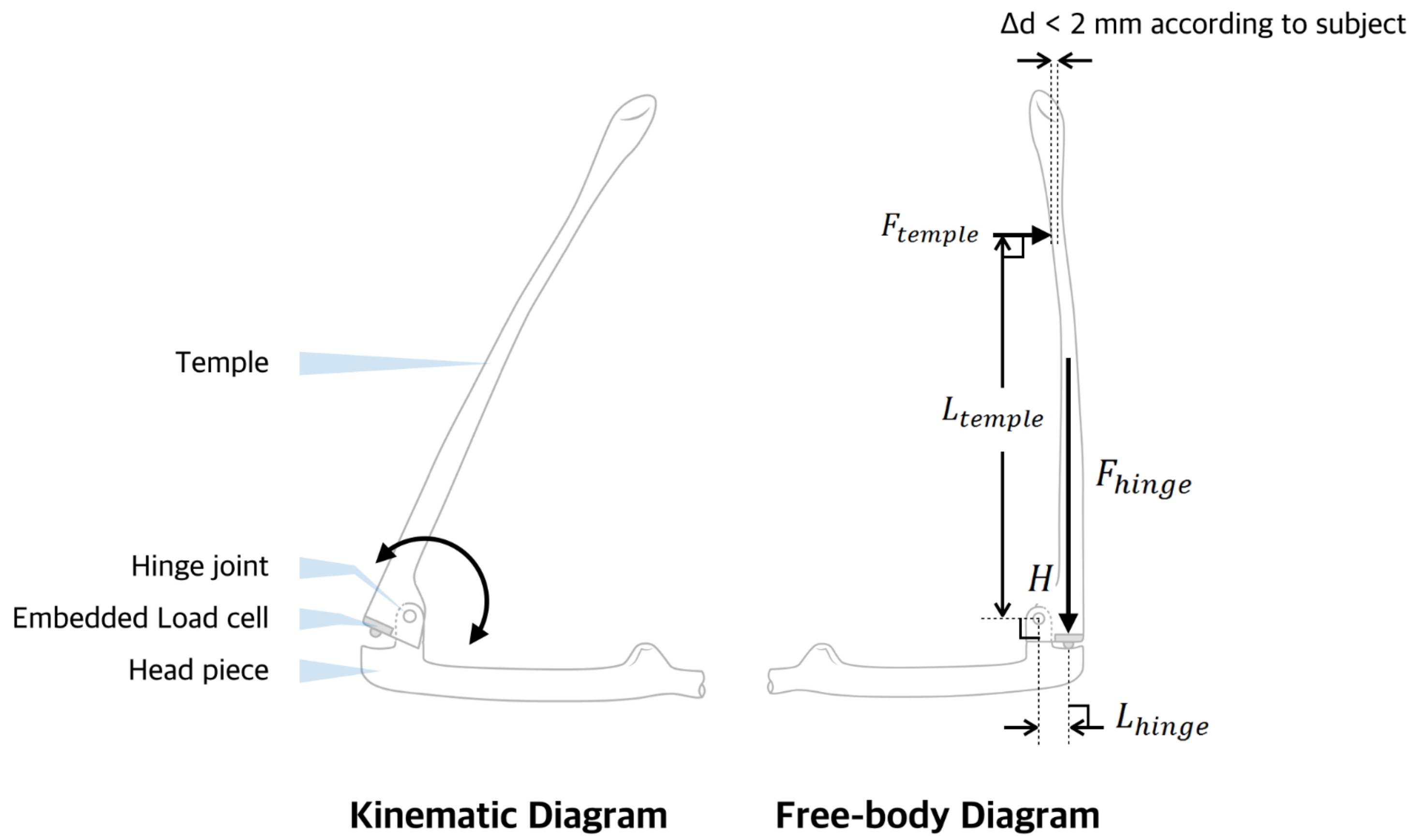

Figure 1.7 Working principle of the system

1.2.3. Monitoring of Ingestive Behavior

Maintaining energy balance in the human body is a vital condition, as abnormal or excessive energy accumulation is the central cause of obesity [9, 10], which could result in various medical complications [11]. The main factors in the energy imbalance are known to be from the both excessive food intake and insufficient physical activity [12]. In 2014, according to an announcement by the WHO, the obesity rate has more than doubled since 1980; further, 39% of adults aged 18 years or older are overweight [13]. These figures indicate that energy imbalance is a worldwide prevalent epidemic; this condition is serious as it can promote many medical complications, such as stroke, heart disease, and cancer [14]. Although its etiology is still incompletely understood, the drastically increasing rate of recent years in modern societies suggests that a behavioral etiology is considered as a significant factor as a biological one [15]; therefore, reduced activity and changes in eating patterns must be monitored continuously over a long time span. Obviously, this behavioral monitoring can also help normal people, who are not suffering from obesity or other eating disorders, in maintaining a healthy life. This study aims to present a device, method, and evaluation for monitoring the food intake at a practical level in daily life.

There have been many discussions on the monitoring of physical activity [16-21], and a variety of commercial products have already been introduced at the consumer level and medical stage [22]. Monitoring of ingestive behavior (MIB), however, has been less studied in practice due to the difficulty of direct and objective measurement of food intake, and is still in laboratory setting since it is difficult to detect the food intake activity in a direct and objective manner. There have been different approaches in the MIB [23-27] such as acoustical approaches based on chewing or swallowing sounds [28-33], morphological approaches sensing deformation of the epidermis [34-39], behavioral approaches using a proximity sensor [40, 41] or an inertia measurement unit (IMU) [42-49], image analysis [50, 51], electrometric approaches analyzing facial muscle activity [52-55], and even pressure information on a smart table [56]. These approaches, however, share common limitations in that they are obtrusive to the eye and intrusive to use in daily life; therefore, we introduce a non-intrusive and un-obtrusive method of direct and objective monitoring of ingestive behavior employing the use of wearable devices. These approaches were also difficult to apply into daily life applications because of their inherent limitations: the methods using sound were easy to be influenced by environmental sound; the methods using the movement of the wrist were difficult to distinguish from other physical activities when not consuming food; and the methods using the image and EMG restricted the boundary of movement and environment. These studies automated the detection of the food intake using sensors, but the scope of the application was limited to the laboratory.

This study utilized the patterns of the temporalis muscle activity as the automatic and objective monitoring of the food intake. The temporalis muscle repeats the contraction and relaxation as a part of masticatory muscle during the food intake [2, 4]; Thus, the food intake activity can be monitored by detecting periodic patterns of the temporalis muscle activity. Recently, there have been several studies utilizing the temporalis muscle activity [7, 57–59], which used the EMG or piezoelectric strain sensor attaching them directly onto the skin. These approaches, however, were sensitive to the location of the EMG electrodes or strain sensor, and were easily detached from the skin due to the physical movement or perspiration. Therefore, we proposed a new and effective method using a pair of glasses that sense the temporalis muscle activity through two load cells inserted in the both hinges in our previous study [60]. This method proved the possibility of detecting food intake with a high accuracy without touching the skin. It was also un-obtrusive and non-intrusive because of the use of the common glasses.

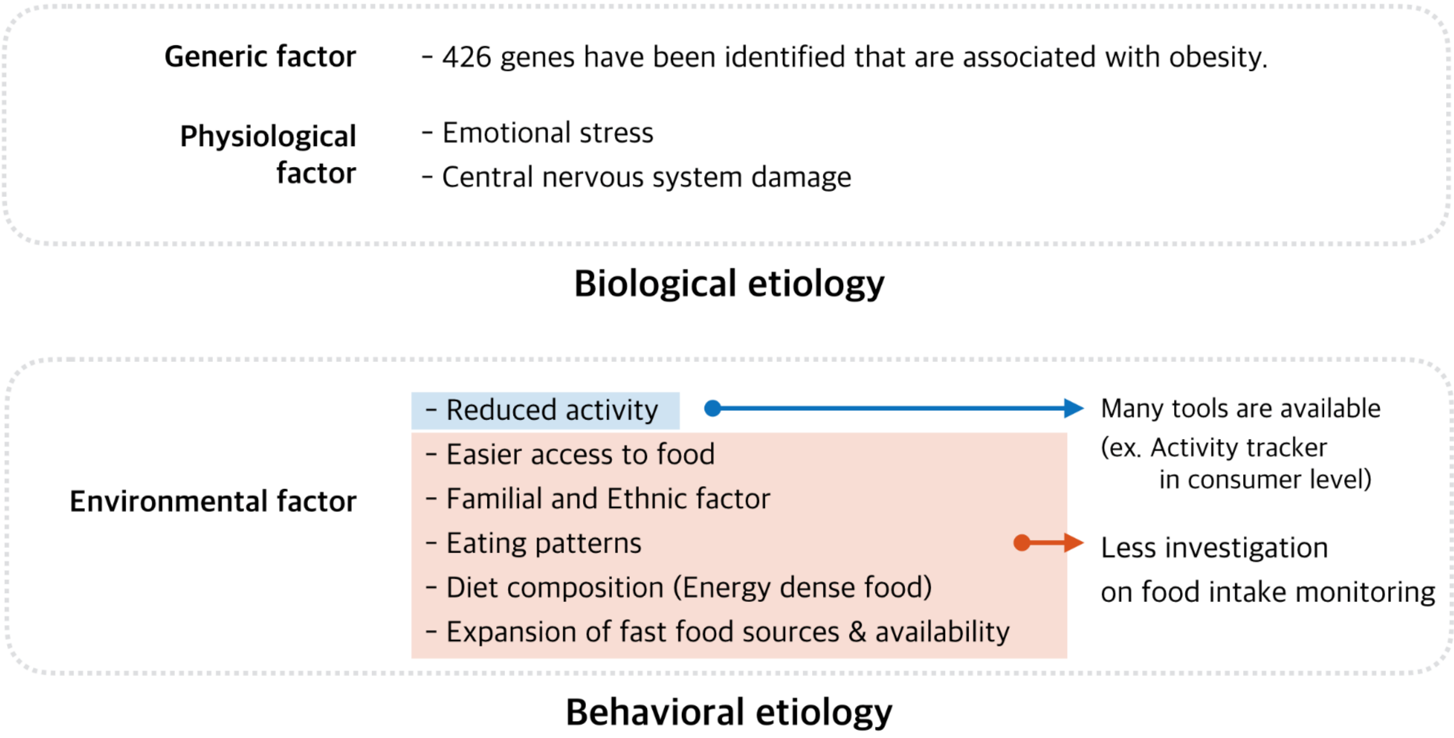

Figure 1.8 Etiology of the energy imbalance

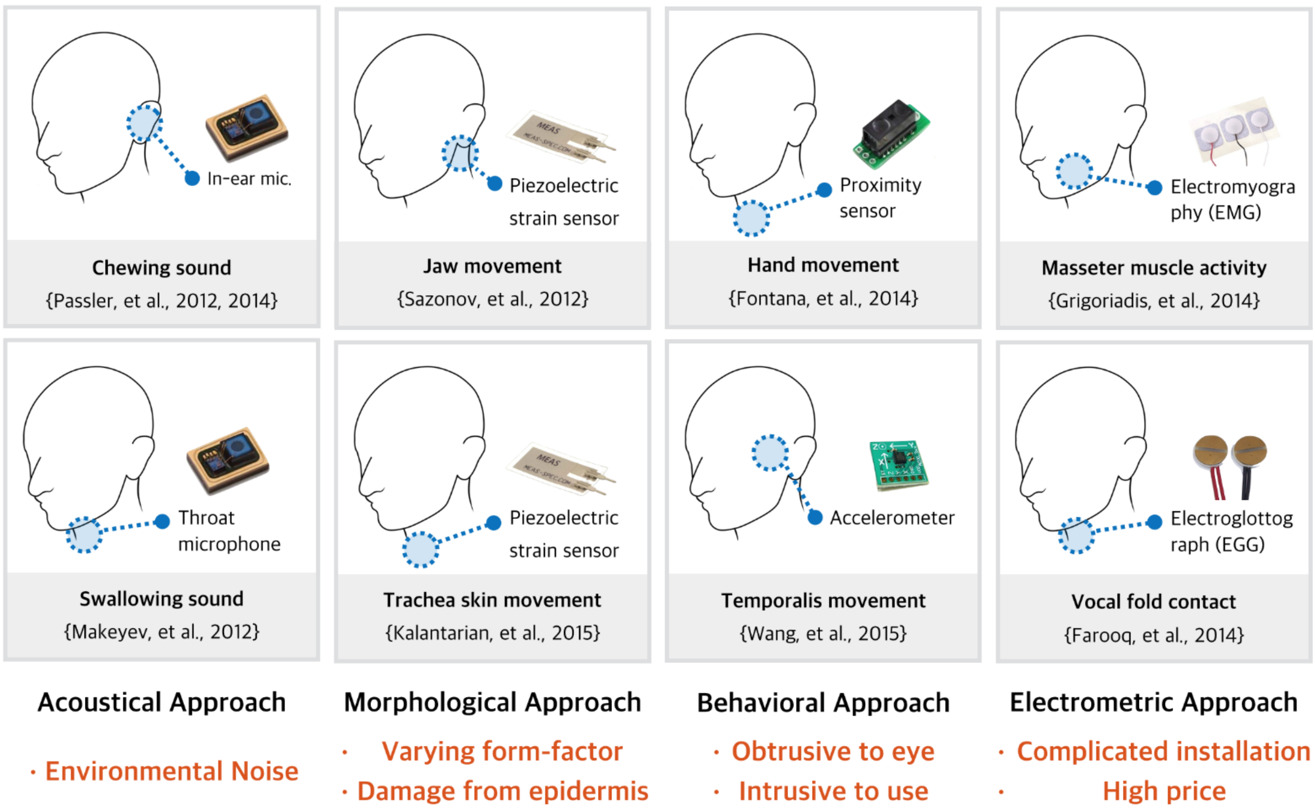

Figure 1.9 Previous approaches on dietary monitoring

1.3. Research Scope and Objectives

In this study, we present a new method for the MIB utilizing the natural lever mechanism of a pair of glasses, named GlasSense. To verity the amplification on the hinge, we conducted an experiment on comparing the force directly exerted on the temple area and its transmitted force on the hinge. In fact, this amplification principle mimics that of sound in the inner ear: the vibration of air (temporalis muscle activity) is amplified by the lever mechanism through the auditory ossicle (temple); and the transmitted force is concentrated on the small stapes footplate area (hinge), compared with the large eardrum area. For practical application, we analyzed left-and-right chewing behaviors and distinguished these from the other facial activity, such as natural head movement, talking and wink. Therefore, six distinct behavior sets from 10 subjects were collected and labeled into the corresponding set: natural head movement (NHM), left chewing (LC), right chewing (RC), left wink (LW), right wink (RW), and talking (TK). Then, algorithms for signal preprocessing, feature extraction, and supervised machine learning were proposed for the classification of the sets.

This study also presents a series of protocols of designing and manufacturing a glasses-type wearable device that detects the patterns of temporalis muscle activities during food intake and other physical activities. We fabricated a 3D-printed frame of the glasses and a load cell-integrated PCB module inserted in both hinges of the frame. The module was used to acquire the force signals, and transmit them wirelessly. These procedures provide the system with higher mobility, for which can be evaluated in practical wearing conditions such as walking and waggling. A performance of the classification is also evaluated by distinguishing the patterns of food intake from those of physical activities. A series of algorithms were used to preprocess the signals, generate feature vectors, and recognize the patterns of several featured activities (chewing and wink), and other physical activities (sedentary rest, talking, and walking).

We also present detailed protocols of how to implement the system that utilized the glasses and temporalis muscle activity for the monitoring of the food intake. This system contains a 3D-printed frame of the glasses, a circuit module, a data acquisition module, and a series of algorithms for data analysis. Furthermore, we also investigated the classification among the featured activities (chewing, walking, and wink) to verify the potential as a practical system, detecting the food intake distinguished from the physical activity.

Chapter 2

Proof-of-Concept Validation

2.1. Experimental Apparatus

We designed 3D-printed frames of a pair of glasses and embedded two ball-type load cells (FSS1500NSB, Honeywell, USA) in one of the temples. One load cell was placed between a gap in the hinge where the temple contacts the headpiece, and the other was on an assumed contact point with the epidermis, which was 69 mm from the hinge joint in this experiment (see Fig. 2.2). The device was fixed to a stage, which had a linearly movable sub-stage to contact the load cell of the temple and a micrometer dial gauge to measure the displacement of the temple. We applied the force to both load cells by moving the sub-stage with a 50 μm resolution.

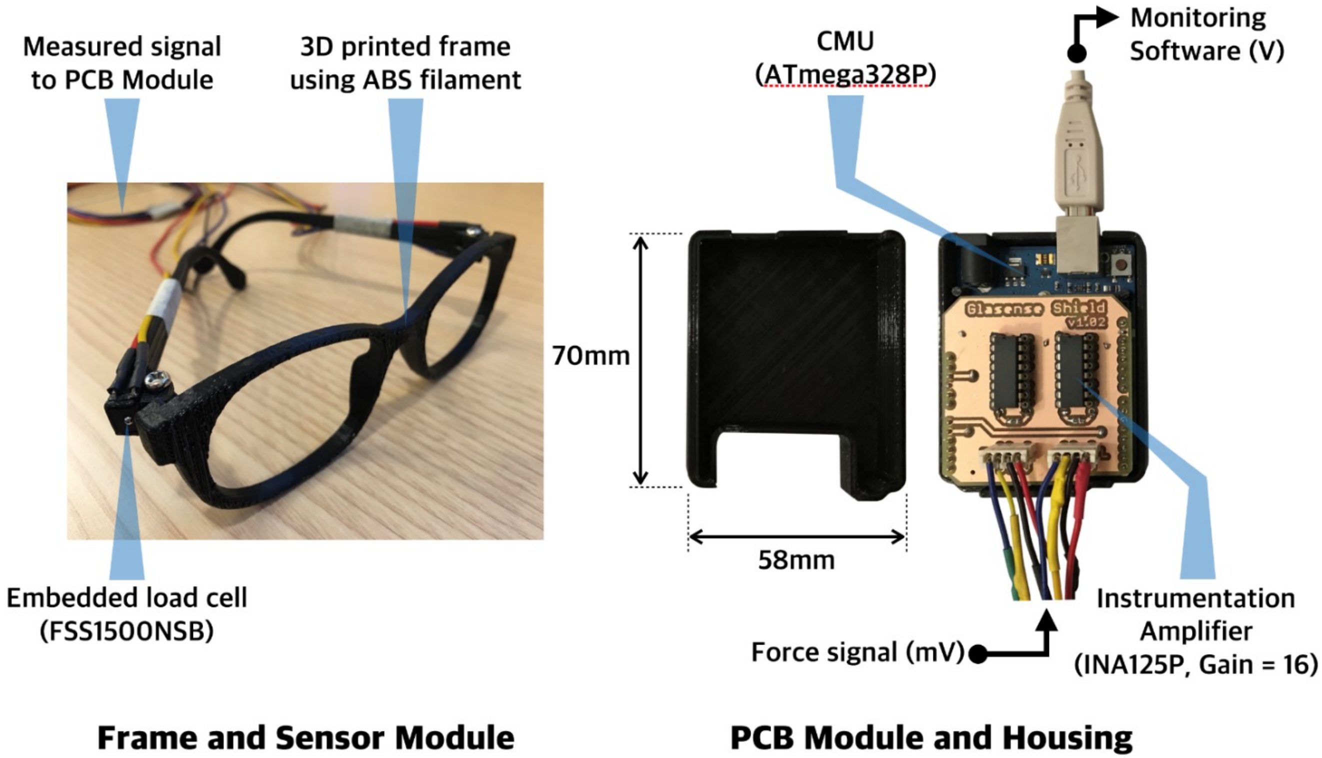

Figure 2.1 Design of the hardware prototype of GalsSense

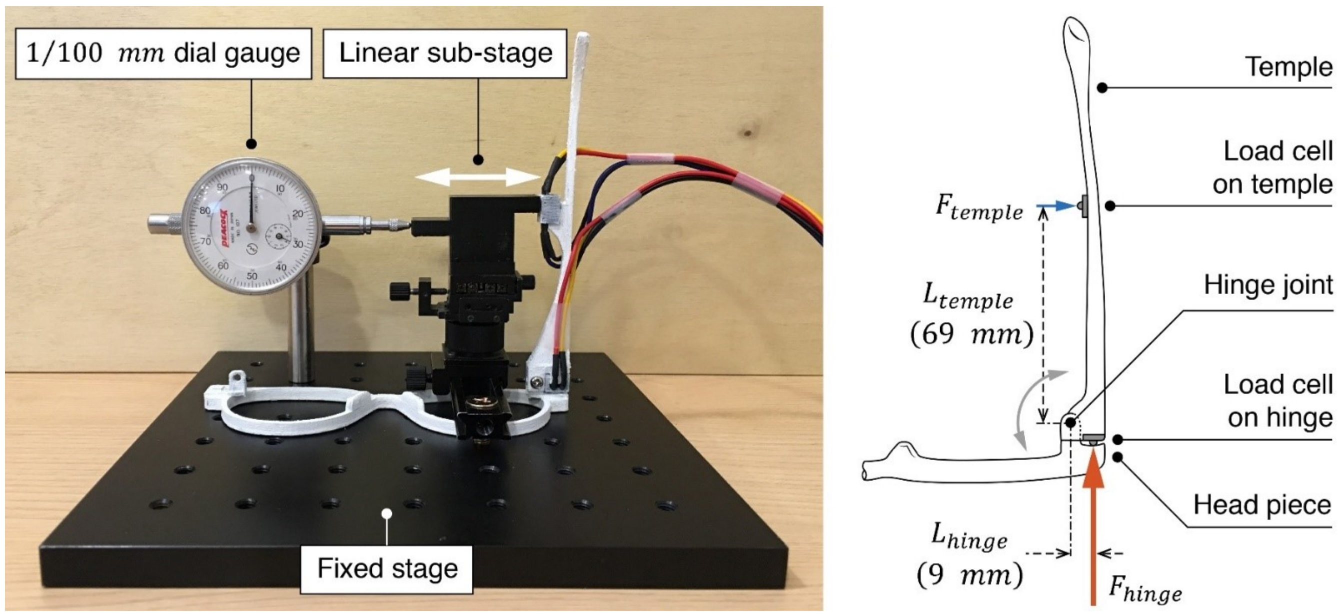

Figure 2.2 Experimental apparatus and dimensions

2.2. Measurement Results

We set a separate experimental apparatus to conduct an objective experiment on the comparison of the forces between the hinge and the temple for the validation of the mechanical amplification. Figure 2.2 shows these settings which were composed of a fixed stage equipped with a linear sub−stage, a micrometer dial gauge, and the glasses. As displacement of the linear sub−stage was changing, the force signal from the hinge, F_{hinge}, showed a large rate of increase in magnitude compared with that from the temple, F_{temple} (Fig. 2.3a). From linear regressions with the least square method which minimizes the sum of squared residuals, we obtained lines−of−best−fit of F_{hinge} and F_{temple}. The both measured force signals showed a high linearity with coefficients of determination of $R^2 = 0.998$ for the hinge and $R^2 = 0.993$ for the temple. The regressions were significant with p−values of $p = 1.53e-121$ for the hinge and $p = 2.43e-95$ for the temple. The slopes calculated from the regression coefficients of the lines−of−best−fit also showed the large rate of increase in magnitude from the hinge (slope = 3.31 N/mm) compared with from the temple (slope = 0.44 N/mm).

Using F_{temple} and F_{hinge} signals as x− and y−values, respectively, we obtained the experimental amplification factor from the regression coefficients (slope) of the line−of−best−fit ($R^2 = 0.997$ and $p = 2.62e-110$); the result showed that the slope was about 7.57, which was almost the same as the theoretical amplification factor, 7.67 (Fig. 2.3b). The theoretical−amplified force is calculated by the moment equilibrium of the temple−hinge joint−head piece system as follows:

$$F_{hinge} = F_{temple} \times (L_{temple}/L_{hinge}) = F_{temple} \times 7.67 \qquad (2.1)$$

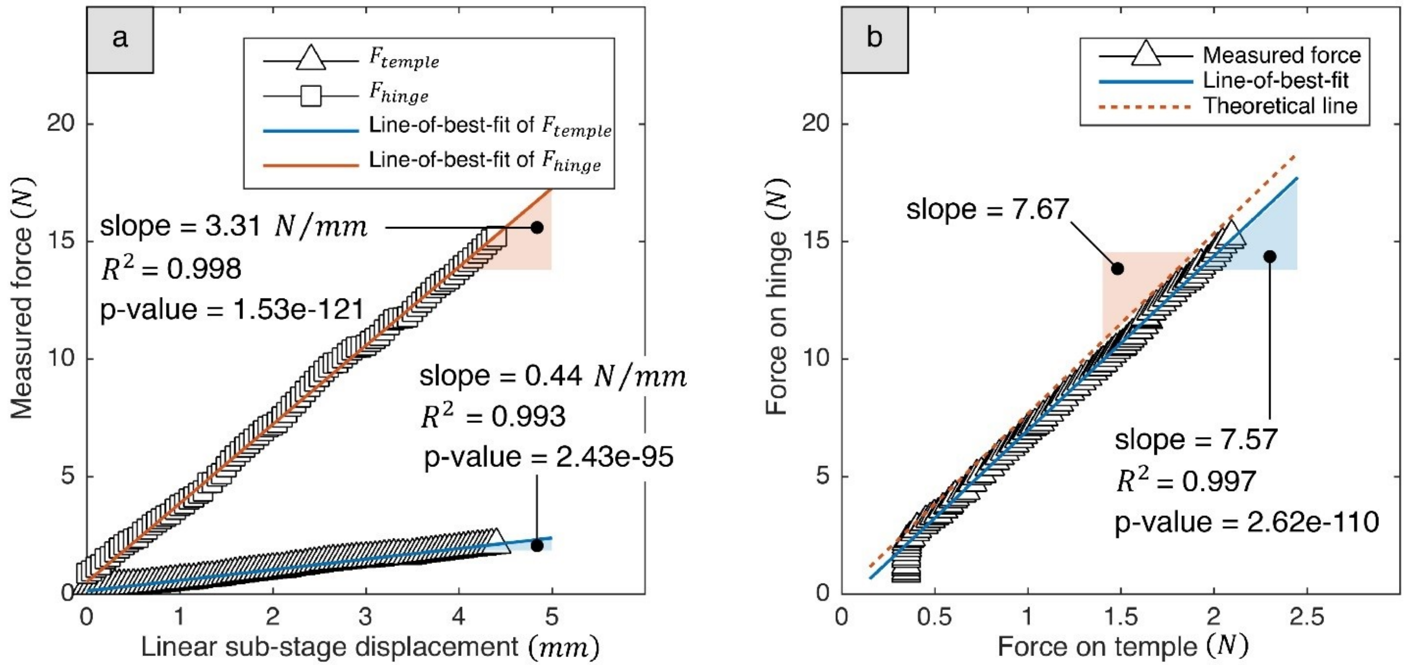

Figure 2.3 Experimental results for the validation of mechanical amplification

2.3. Discussion

In this study, we aim to present a novel method to sense temporalis muscle activity through load-cell-embedded-glasses, GlasSense. Utilizing the natural lever mechanism between the temple and the head piece, we obtained an amplified and concentrated force on the hinge. This mechanical amplification was verified by comparing the force between the temple and the hinge (Fig. 2.3). The experimental amplification factor, 7.57, showed almost the same value as the theoretical one, 7.67. It is expected that the slight decrease in the experimental value was due to measurement errors and other reaction forces in the real world, such as friction of the hinge joint. With the exception of such factors, the amplification factor is purely influenced by the geometric properties, L_{temple} and L_{hinge}, according to the moment equilibrium equation (2.1). So, we can increase the amplification factor by increasing the proportion of L_{temple} to the L_{hinge} as much as possible.

When the exerted force on the temple was smaller than 0.5 N, a large deviation of the data from the line-of-best-fit was observed as shown in Figure 2.3b. We assume two possible reasons: the contact and the exerted force were insufficient to measure the meaningful data in this condition (< 0.5 N); and weight of the temple and the electronic wires primarily affected the load cell on the hinge when the applied force was extremely small. When enough forces greater than 0.5 N were exerted on the temple, the experimental results were in a good agreement with simulation results for amplification factors. In general wearing condition, these gravitational and contactless factors can be discarded because the glasses is equipped with the perpendicular direction to the gravity, and the sensors have pre-loaded compressive force enough to support the glasses against the gravity.

In practical wearing situation, the difference in the contact area between the temple and the hinge also affect the amplification factor. The contact area of the temple is larger than that of the hinge and differ from individual to individual. The transmitted force to hinge, meanwhile, can be concentrated and accommodate a variety of individual's form factors. With the consideration of the force concentration, the amplification factor is expected to become much larger than the experimental result.

Chapter 3

Implementation of GlasSense

3.1. Hardware Prototyping

As this study focuses on a data analysis to distinguish the food intake from other physical activities such as walking, the sensor and data acquisition system need to be implemented to provide mobility. Thus, the system includes two load cells, two amplifiers, a micro controller unit (MCU) with wireless communication capability, and a battery.

3.1.1. Preparation

In this step, we prepare electronic parts to manufacture a sensor-integrated and data-transmitting circuit module of GlasSense.

Load cells

We prepared two load cells to measure force signals on both the left and right sides of the glasses. In this study, two ball-type load cells (FSS1500NSB, Honeywell, USA) was used. This force sensor operates in a range between 0 N and 15 N, and produces an output of low differential voltage with maximum 120 mV span in a 3.3 V excitation. Thus, the amplification of the output voltage is needed to implement the protocol.

Instrumentation Amplifier

We prepared two amplifiers to magnify each force signal of the load cells, respectively. Two instrumentation amplifiers (INA125U, Texas Instruments, USA) were used to obtain an accurate and stable output voltage. The gain-setting resistor R_g was set to 15 kΩ, thereby it amplifies the force signals eight times, up to 960 mV, not to exceed a 10−bit analog−to−digital converter (ADC) of the micro controller unit (MCU) we used in the next step.

Micro controller unit

We prepared an MCU to read the force signals and to transmit them to a data acquisition module wirelessly. The ESP8266 module (ESP−07, Shenzhen Anxinke Technology, China) was used to utilize the both 10−bit ADC and Wi−Fi connectivity. Note that we have two analog force inputs; we need to use a multiplexer in the next step, however, since the ESP8266 series have only one analog input pin.

2−channel multiplexer

We prepared an analog multiplexer to handle the two signals with one ADC pin. A two−channel multiplexer (74LVC1G3157, Nexperia, Netherlands) was used.

Lithium−ion polymer battery

We prepared a battery to operate the system during an experiment. A lithium−ion polymer (LiPo) battery (MP701435P, Maxpower, China) were used with a 3.7 V nominal voltage, 300 mAh nominal capacity, and 1 C discharge rate. As the entire circuit system consumes maximum 200 mA per hour when transmitting data, the battery was chosen to supply enough current per hour more than 200 mAh.

Other parts

We prepared five 12 kΩ registers as pull-up resistors of the ESP-07. The surface-mounted devices (SMD) type resistors of 2012 metric size were used.

3.1.2. Load Cell-Integrated Circuit Module

Figure 3.1 and 3.2 show the schematic diagram of the left and right circuit, respectively. Autodesk EAGLE was used for the circuit design and the fabrication of the circuit boards. Figure 3.3 show the results of the left and right board artworks, respectively. In order to reduce the size and weight of the system and obtain a reliable quality, we placed an order of the fabrication process to a PCB fabrication company in South Korea. We soldered every electronic component prepared in chapter 3.1.1 of the protocol to the PCBs. In Figure 3.4, the complete version of the both top and bottom layers of the both boards are presented. Note that INA125 series is very sensitive to the soldering temperature. Make sure that lead temperature does not exceed 300°C for 10 seconds during soldering, otherwise it may cause the permanent damage to the component.

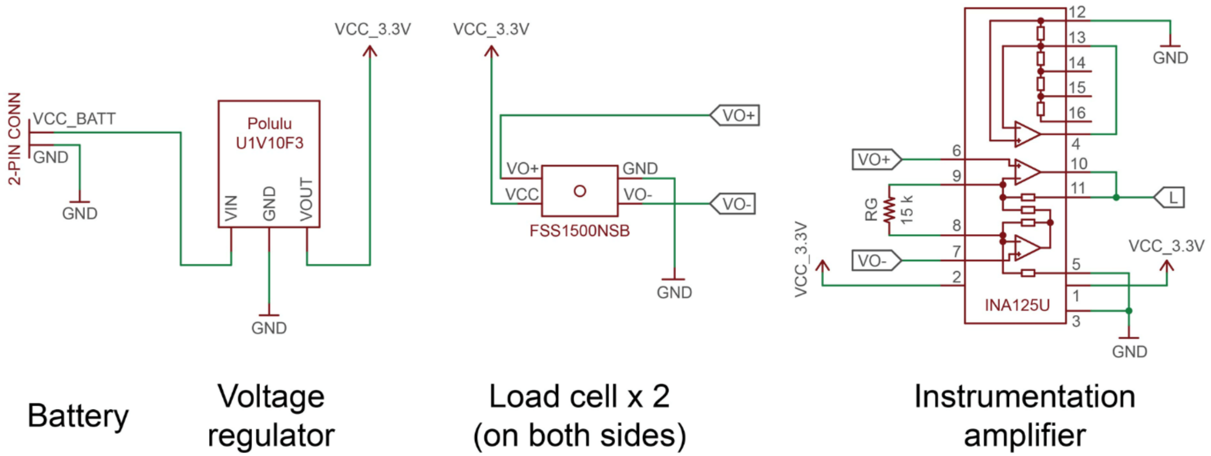

Figure 3.1 Schematic diagram of the left circuit modules

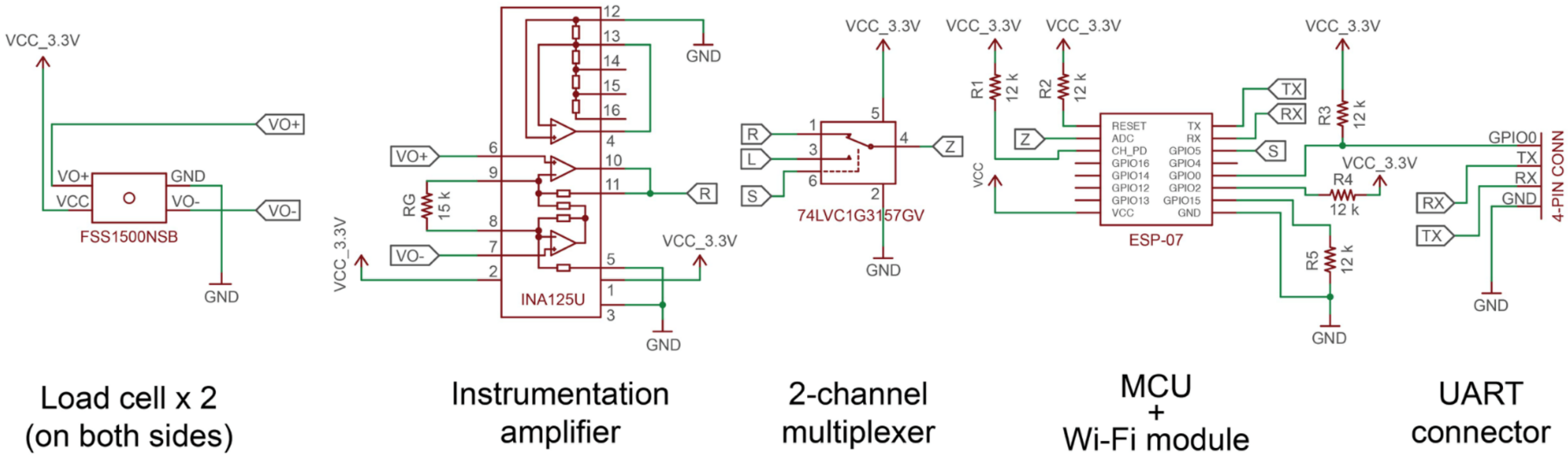

Figure 3.2 Schematic diagram of the right circuit module

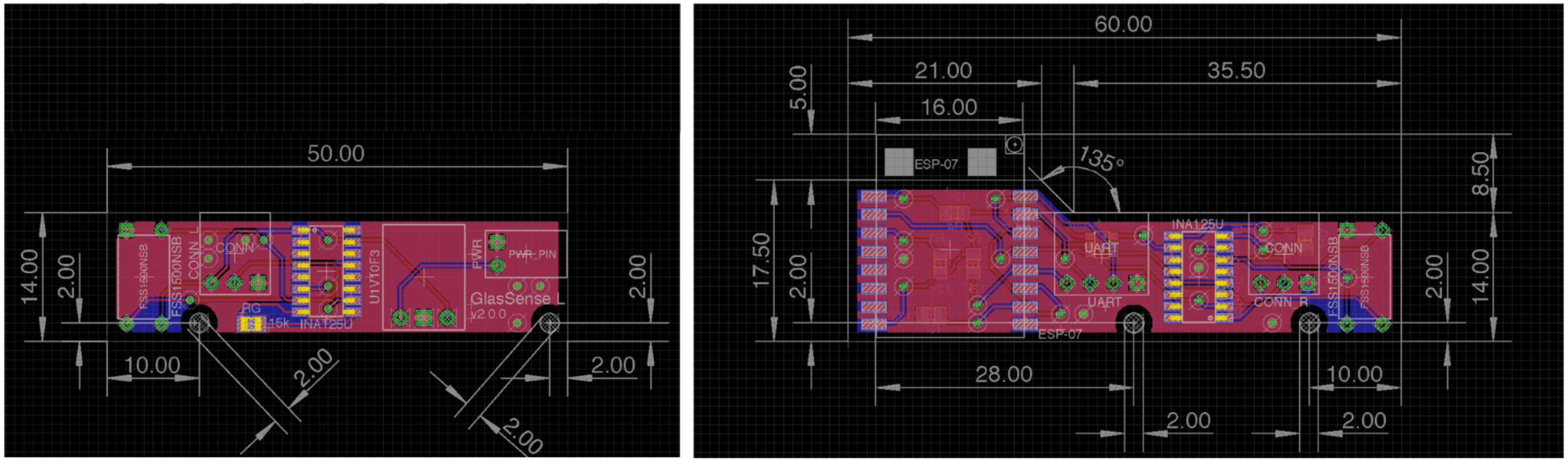

Left Board **Right Board**

Figure 3.3 PCB artworks of the left and right circuit boards

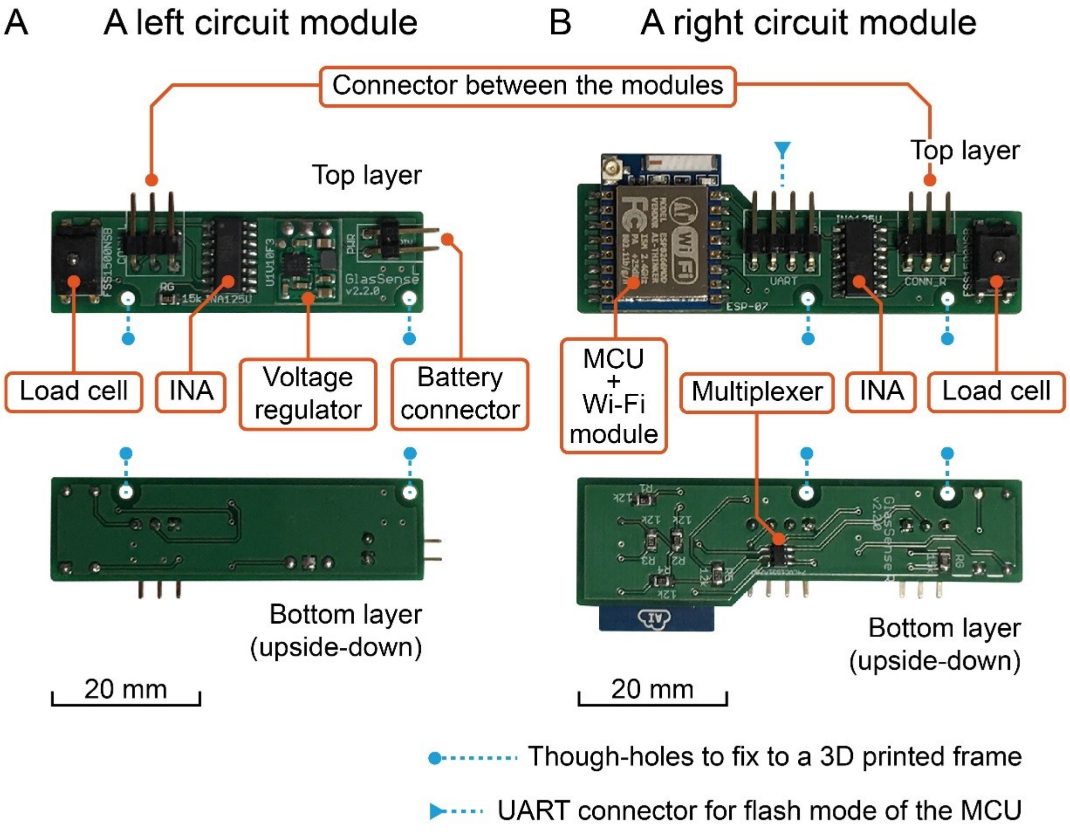

Figure 3.4 PCBs soldered with all electrical components

3.1.3. 3D Printed Frame of Glasses

The frame consists of a head piece and a pair of temples on both sides.

Head piece design

We designed a 3D model of the head piece of the glasses using a 3D modeling tool as shown in Fig. 3.5a. We used the Autodesk Fusion 360 for modeling. Any commercial 3D design tools can be replaced for it.

Temples design

We design the 3D model of the left and right temples of the glasses as shown in Fig. 3.5b and Fig. 3.5c. The temple parts should be designed to integrate the PCB modules fabricated in section 3.1.2 of the protocol. The load cell should be placed to be pressed by a support bolt at a support plate of the head piece when equipped.

3D printing

We printed the head piece and temple parts using a 3D printer (Ultimaker 2, Ultimaker, The Netherlands) and a carbon fiber filament (ColorFabb XT-CF20, ColorFabb, The Netherlands) at 240°C of a nozzle temperature and 80°C of a bed temperature. The use of any commercial 3D printer and any types of filaments such as ABS and PLA can be permitted. The nozzle and bed temperatures may be adjusted according to the filament and printing conditions.

Polishing

The tips of the temples were heated using a hot air blower of a 180°C setting and bend them inward like conventional glasses. The degree of bending does not need to be rigorous as the purpose of the curvature is to increase a form factor by helping the glasses fit on a subject's head when equipped. Be careful, however, that excessive bending will prevent the temples from touching the temporalis muscle, which makes it impossible to collect significant patterns.

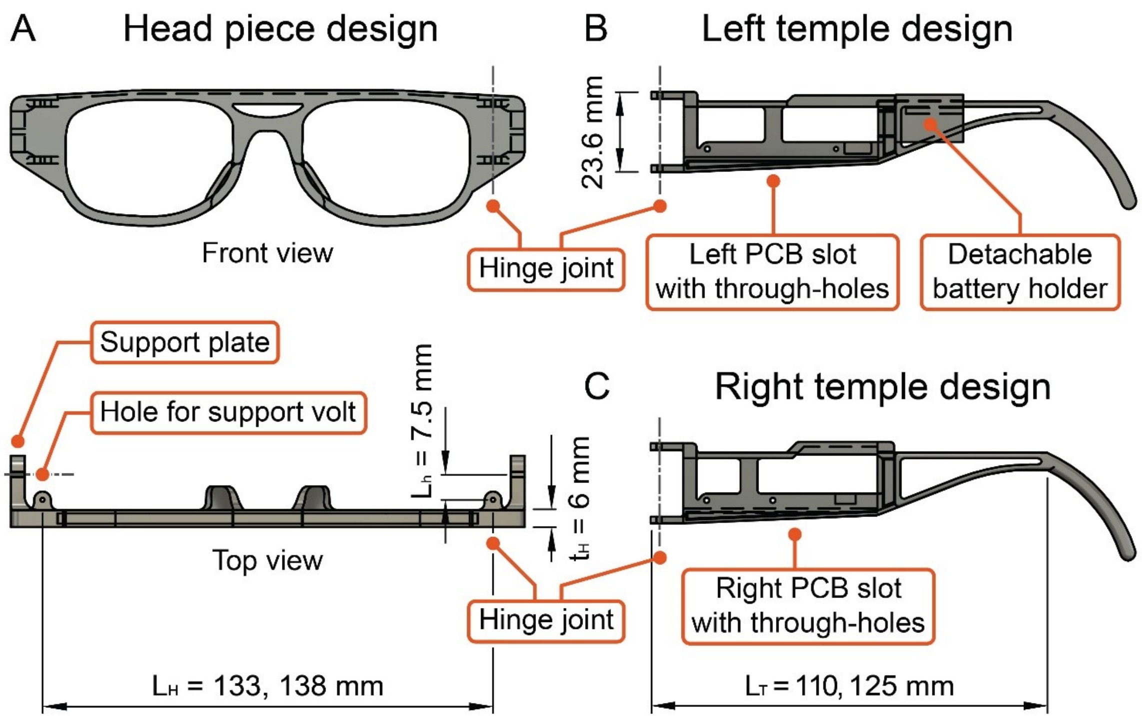

Figure 3.5 Design of 3D models of the glasses

3.1.4. Hardware Integration

We inserted the PCB modules into the temples by using M2 bolts to fasten it. A representative result of the PCB−integrated glasses was shown in Fig. 3.6. Then, we assembled the head piece and the temples by inserting the M2 connecting bolts into the hinge joints. After that we connected the left and right PCBs using the connecting wires. Finally, the battery was connected to the left circuit and attached to the left temple. The mounting side of the battery is not critical, since it may vary depending on the PCB design. We also covered rubber tapes on the tip and the nose pad of the glasses to add more friction with the human skin as shown in Fig. 3.6.

Through the procedures outlined above, we prepared two versions of the 3D printed frame by differentiating the length of the head piece, L_H (133 and 138 mm), and the temples, L_T (110 and 125 mm), as shown in Fig. 3.5. Therefore, we can cover various wearing conditions which can be varied from subjects' head size, shape, etc. The subjects chose one of the frames to fit it to their head in the user study. The vertical distance, L_h, between the hinge joint and the hole for the support bolt was set to 7.5 mm for the amplified force not to exceed the 15 N, the linear operating range of the load cell. The head piece should have a thickness, t_H, enough to resist the bending moment transmitted from the both support bolts when equipped. We chose the t_H to be 6 mm with a use of carbon fiber material from a heuristic approach. The contact points can be adjusted through the support bolts to fine−tune the tightness of the glasses as shown in Fig. 3.7.

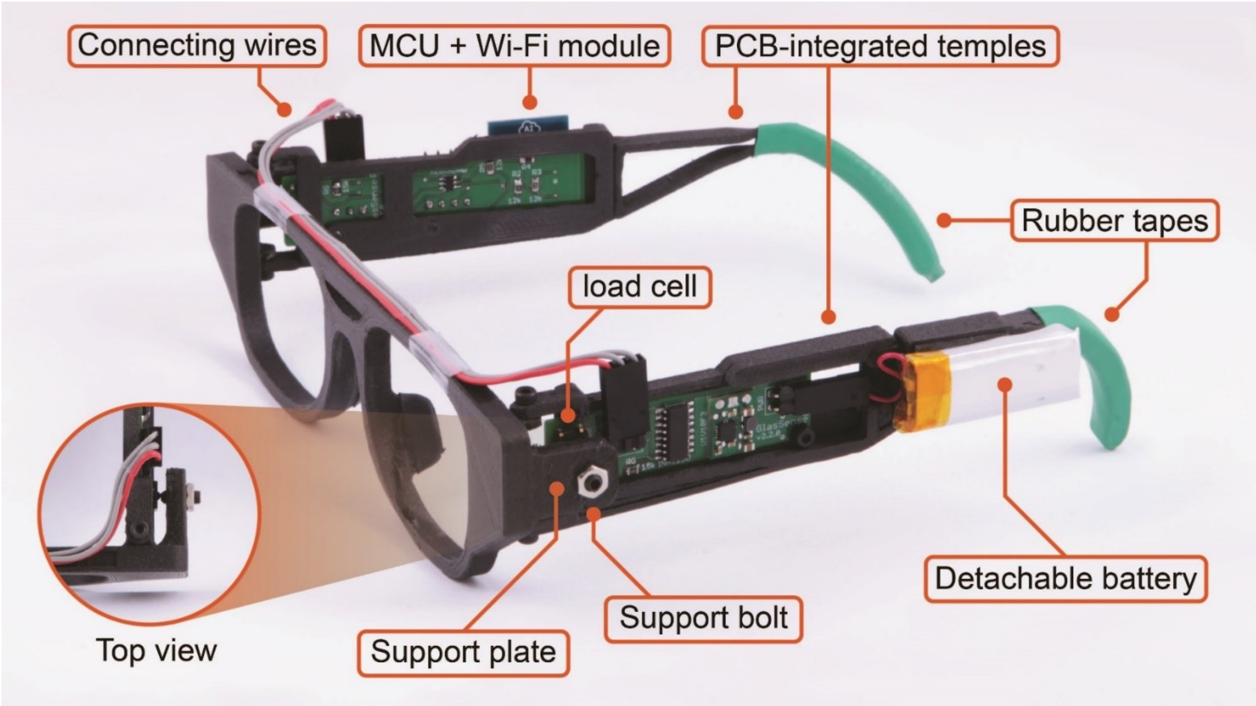

Figure 3.6 A PCB−integrated GlasSense

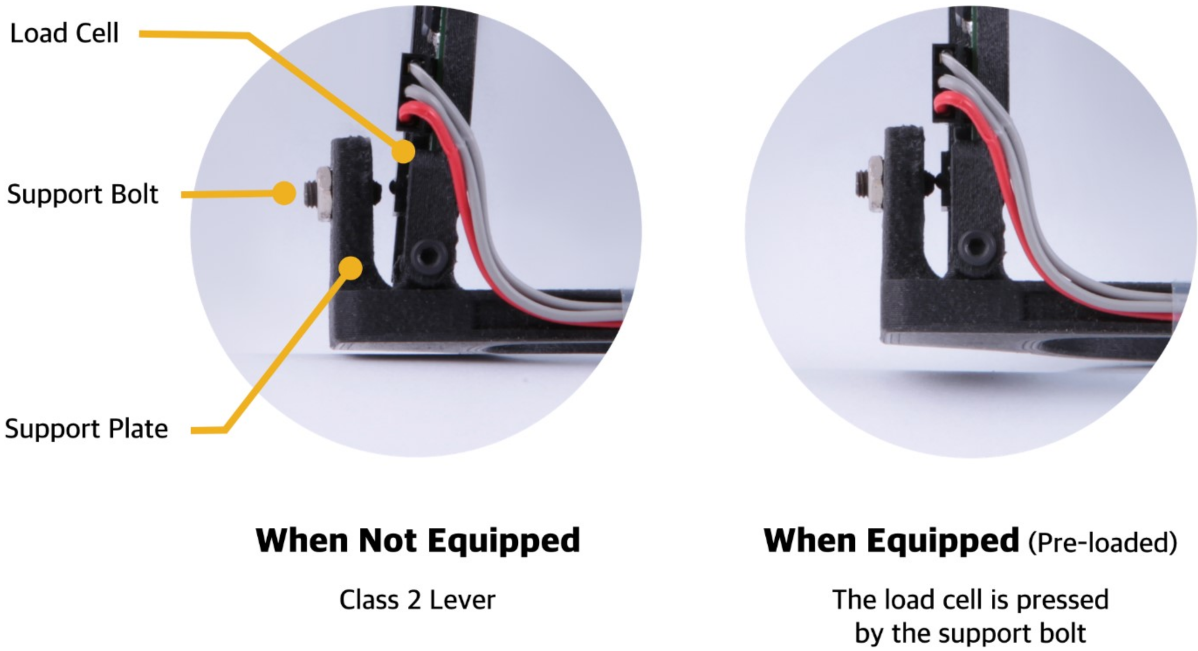

Figure 3.7 Detailed structure of hinge

3.2. Data Acquisition System

The data acquisition system is composed of a data transmitting module and a data receiving module. The data transmitting module read the time and the left and right force signals, and then send them to the data receiving module, which gathers the received data and write them to a file.

3.2.1. Wireless Data Transmission

We generated the codes which read the time and force signals with 200 samples per second, and transmit them to the data receiving module. We make the ESP-07 act as an access point (AP) and send the data through a user datagram protocol (UDP) stream. Arduino IDE was used to develop the codes.

3.2.2. Data Collecting Module

We also generated the codes which receive the transmitted data and save them to a file. The received data is saved with a subject's information such as name, sex, age, and body mass index (BMI). We used Unity IDE and C# with MonoDevelop to develop the codes. Build the generated codes into a smart phone. In this study, we used iPhone 6s Plus (Apple, USA), but any computing device (Android, Windows, OSX, etc.) is allowed if it has a Wi-Fi capability.

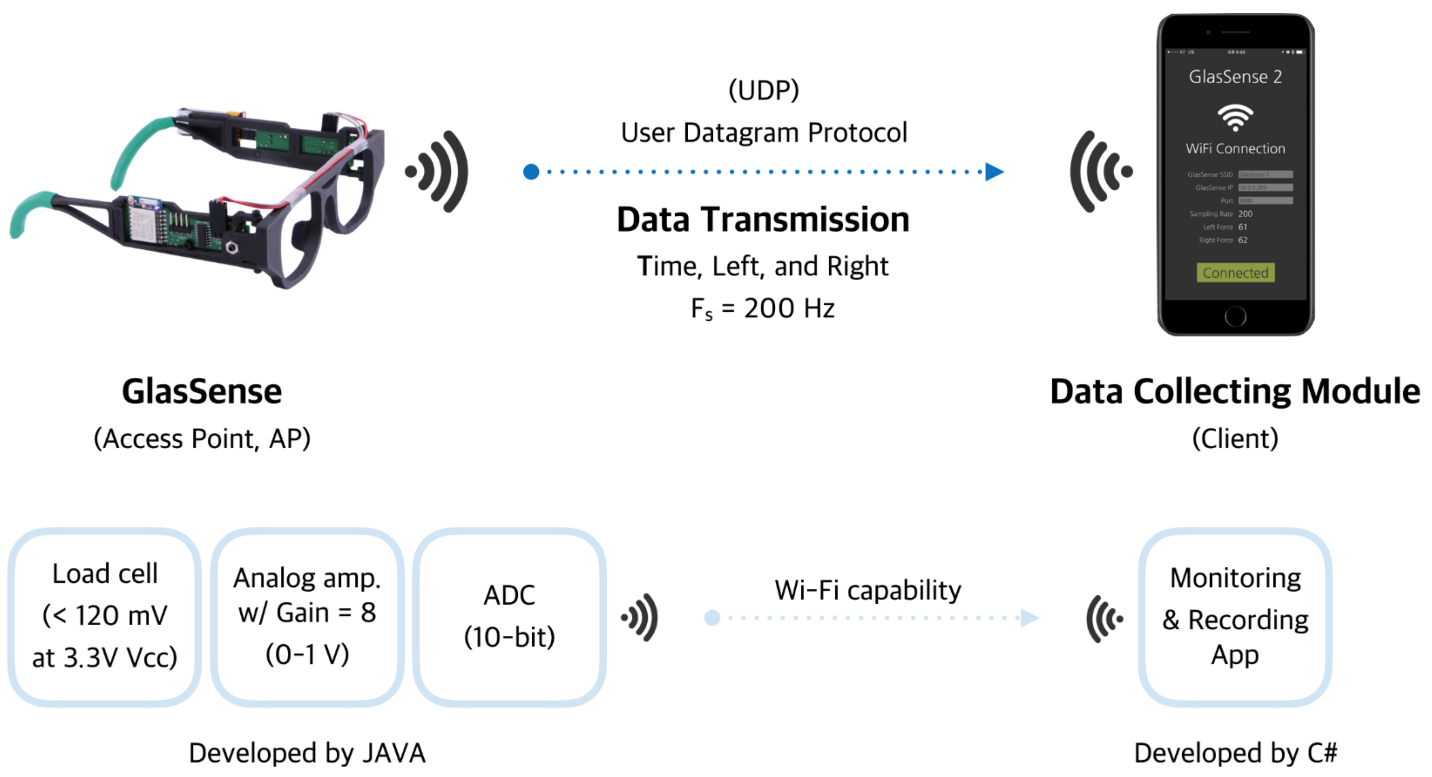

Figure 3.8 Scheme of data acquisition system through wireless capability

Chapter 4

Data Collection through User Study

4.1. Preparation for Experiment

In this study, all the experiments were performed by simply wearing the glasses. All the data were acquired by measuring the force signals from load cells inserted in the glasses and not in a direct contact with the skin. All the procedures including the use of human subjects were accomplished by a non–invasive manner of simply wearing a pair of glasses as usual. The data were wirelessly transmitted to the data recording module, which, in this case, a designated smart phone for the study. All the protocols were not related to *in vivo/in vitro* human studies. No drug and blood samples were used for the experiments. Informed consent was obtained from all subjects of experiments.

Before starting the user study, a subject selected a pair of glasses which have an appropriate size and form factors to the head. Then, fine−tune of the tightness with the support bolts at both the hinges was provided (Fig. 3.7). Note that the force values must not exceed 15 N, since the force sensors suggested in this study may lose the fine linear characteristic in case of 15 N input force. After all the preparation for the experiment, the six featured activity sets were collected: sedentary rest (SR), sedentary chewing (SC), walking (W), chewing while walking (CW), sedentary talking (ST), and sedentary wink (SW).

4.2. Activity Recording

The purpose of this study was to design a pair of glasses and define a classifier model that consistently sense temporalis muscle activity regardless of intra- and inter-individual variability. Thus, we collected and analyzed the data from 10-subject user study (five males and five females, the average age was 28.2 ± 3.3 (s.d.: standard deviation) years, ranged at 22–31 years, and the average body mass index (BMI) was 21.4 ± 3.5 (s.d.) kg/m^2, ranged at 17.9-27.4 kg/m^2) to define only one SVM classifier corresponding to all subjects. We recorded force signals per every consecutive window of 2-second frame. This window size was chosen from the fact that chewing frequency mainly ranges from 0.94 Hz (5th percentile) and 2.17 Hz (95th percentile) [61]. So a 2-second single window could contain multiple chewing activities. In order to reflect the variety of food properties, the chewing sets were conducted for three different food textures: bread (sliced white breads and croissants); potato chip (Lay's); and jelly (Jelly Belly). Each item differentiates its texture from a distinct hardness, crispiness, and tackiness. For example, the bread represents the soft, the potato chip does the hard and crispy, and the jelly does the soft and tacky texture. The toasted bread was served in slices of 20 mm by 20 mm size good for eating. In the case of SW, we informed the subjects of the timing of wink by an informing bell sound of 0.5 seconds long every three seconds.

We recorded an activity during 120-second block and generate a recording file of it. This file contains a sequence of the time when the data was received, a left force signal, a right force signal, and a label representing the current facial activity. Visualizations of temporal signals of all activities in a block of a user were depicted in Fig. 4.1. The six featured activity sets (SR, SC, W, CW, ST and SW) were labeled as 1, 2, 3, 4, 5, and 6, respectively. The labels were used to compare the predicted classes in section 8 of the protocol.

We provided a 60-second break after the recording block. The subjects took off the glasses during the break, and wore it again when the recording block restarted. This action prevents the data from being overfit to a specific wearing condition. We repeated the block-and-break set four times for each activity. In the case of SC, SW, and W, the subjects conducted the blocks in the order of left, right, left, and right, sequentially. We also repeated the block-and-break sets for all the activity sets.

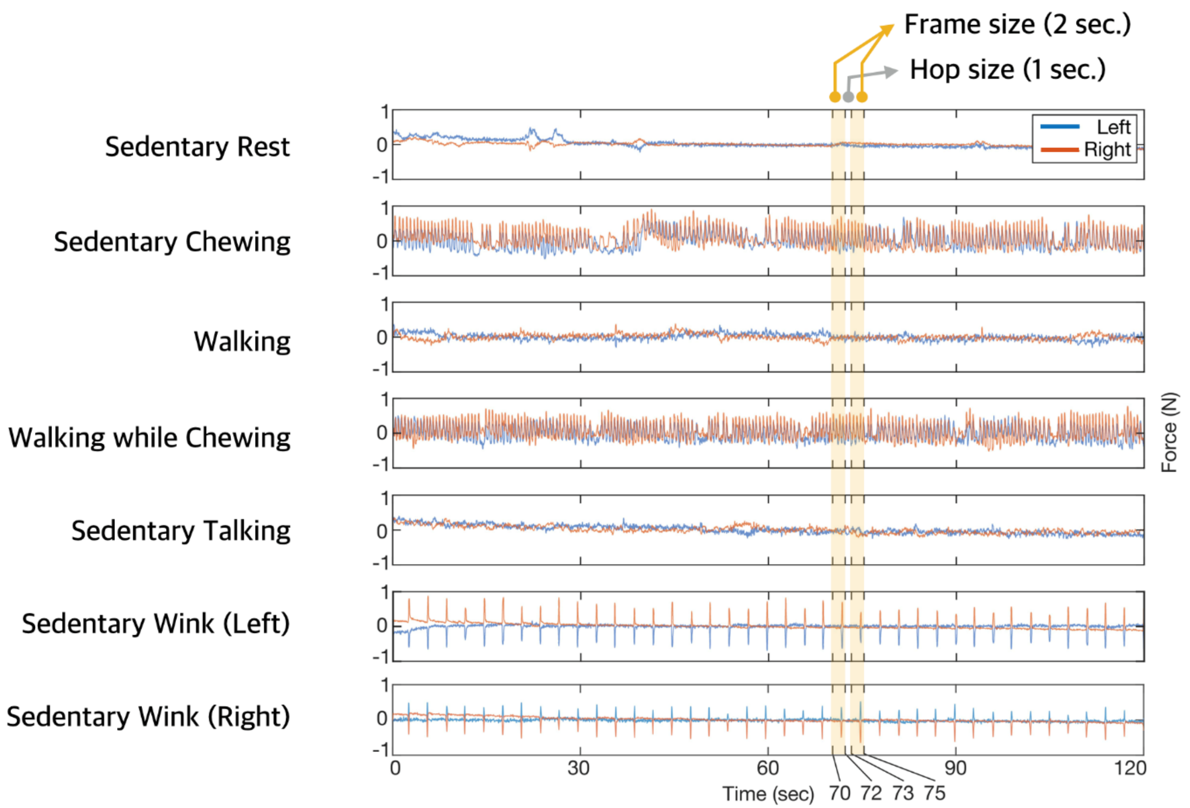

Figure 4.1 Temporal signal of a recording block

Chapter 5

Feature Extraction

5.1. Signal Preprocessing and Segmentation

In order to classify the collected samples into the corresponding sets, we applied a series of algorithms for signal preprocessing, feature extraction, and supervised machine learning techniques. First, the Hanning window was applied to each window to reduce the spectral leakage on performing the FFT. A low-pass filter with cut-off frequency of 10 Hz was then applied to calculated power spectral density (PSD) functions, because the chewing frequency does not exceed 3 Hz [61]. From the Figure 5.2, it was confirmed that the frequency higher than 10 Hz had too small variation among the sets to use for classification.

The left and right signals are calculated separately in the following procedures. All the procedures were implemented in MATLAB (Mathworks, U.S.A.).

5.1.1. Temporal Frame

We segmented the recorded signals into frames of two seconds long by hopping them at 1-second intervals as shown in Fig. 4.1. Apply a Low-Pass Filter (LPF) using a 5^{th} order Butterworts filter with a cutoff frequency of 10 Hz for each frame. The results were saved as the temporal frames for the next steps.

5.1.2. Spectral Frame

We subtracted the median value from the original signals of a frame to remove the preload when equipped with the glasses. The preload value is not required for the following frequency analysis, since it does not include any information about chewing, walking, wink, etc. On the other hand, it connotes insignificant information, which can vary from subject to subject, from every setting of the glasses, and even from the moment a subject wear the glasses. We applied the Hanning window to each frame to reduce a spectral leakage on frequency analysis. A single-sided spectrum use produced by applying a Fast Fourier Transform (FFT) to each frame. A combination of a temporal frame and a spectral frame of the same time was defined as a frame block or simply a frame.

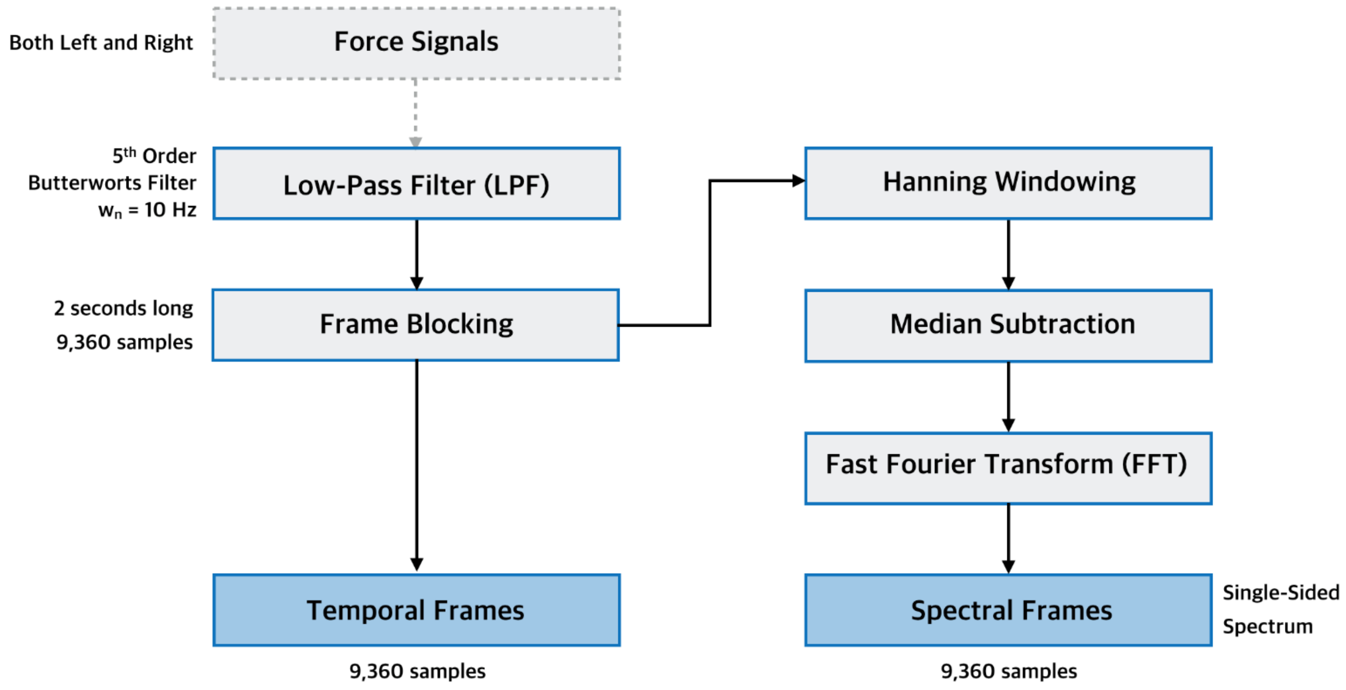

Figure 5.1 Block diagram on signal preprocessing and segmentation

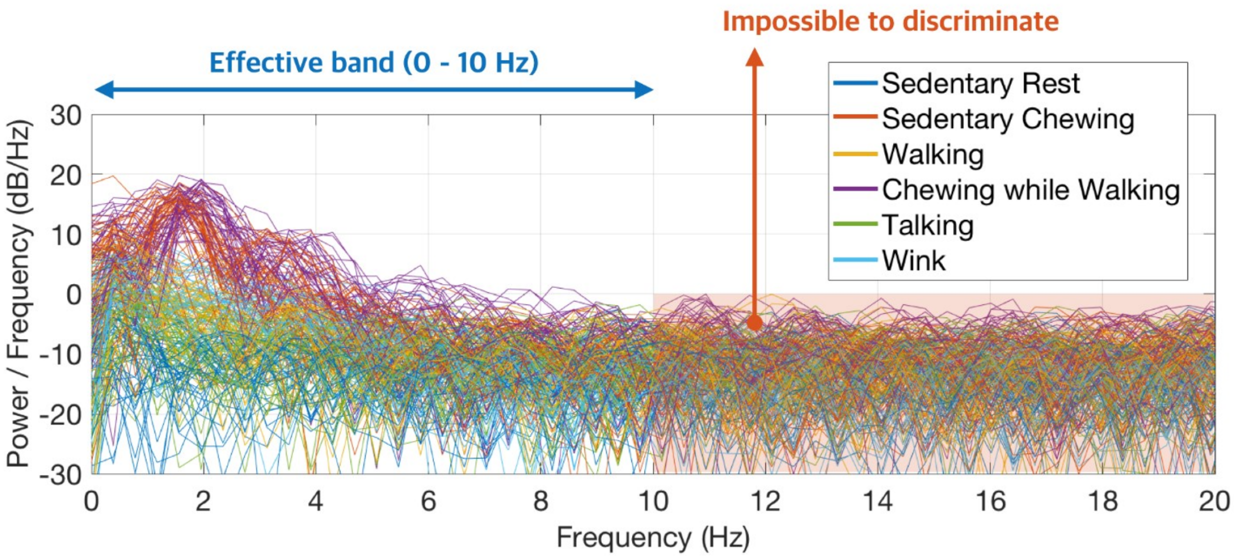

Figure 5.2 Power spectral density (PSD) functions of all activities

5.2. Feature Extraction

In this study, the signals were related to time series analysis, such as audio signal, EMG signal, inertial signal, etc. Because these data is voluminous and dynamic, it is hard to process directly in any analysis task. Time-domain and frequency-domain features have representative information of the original signals and reducing the volume of data [62].

A feature vector is generated per frame produced in chapter 5.1. The left and right frames are calculated separately and combined into a feature vector in the following procedures. All the procedures were implemented in MATLAB.

In order to extract appropriate features for the classification, we used statistical features from temporal and spectral domains of a window (2-second recording frame). The entire feature list can be found in Tables 5.1 and 5.2. Total number of 84 features was used to build a feature vector with a label ranged from 1 to 6 depending on its behavioral set.

After that, we extracted statistical features from both temporal and spectral domains. The temporal features were calculated from the filtered force signals and the spectral features from a single-sided spectrum of the FFT. The left and right features were calculated separately except for correlation features such as a correlation coefficient and signal magnitude area. The correlation of the left and right force signals enabled the classification of the LC and RC. These features were then scaled and normalized over the whole feature vectors. After that, an 84-dimensional feature vector and the corresponding label were created for each sample. Finally, this feature vector and label were used to train and predict the class using Support Vector Machine (SVM), a well-known classifier that shows excellent performance in generalization and robustness on supervised machine learning problems [63]. In this study, we used the LibSVM [64] software package for MATLAB to implement the SVM classifier with a Radial Basis Function (RBF) kernel.

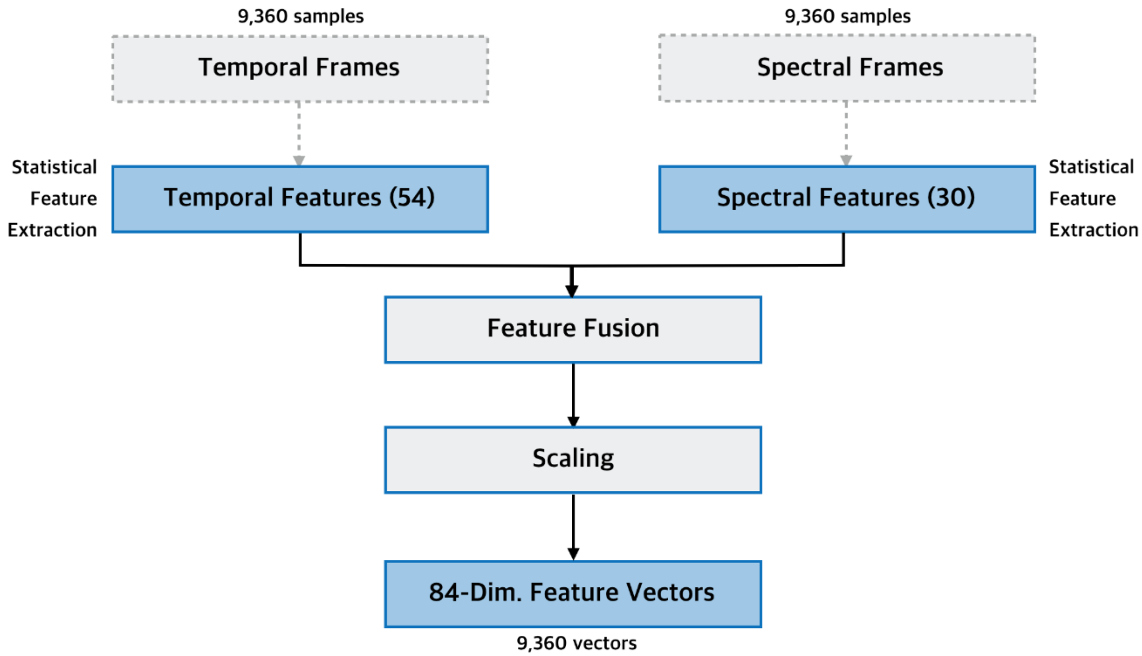

Figure 5.3 Block diagram on feature extraction

5.2.1. Temporal Features

We extracted statistical features from a temporal frame. A list of the total number of 54 features is given in Table 5.1.

Table 5.1 A list of extracted temporal features

No.	Feature description	No.	Feature description
1	Standard deviation L	28	Skenwness R
2	Standard deviation R	29	Kurtosis L
3	Coefficient of variation L	30	Kurtosis R
4	Coefficient of variation R	31	Autocorrelation function coefficients L
5	Zero crossing rate L	32	Autocorrelation function coefficients R
6	Zero crossing rate R	33	Signal energy L
7	20th percentile L	34	Signal energy R
8	20th percentile R	35	Log signal energy L
9	50th percentile L	36	Log signal energy R
10	50th percentile R	37	Entropy of energy L
11	80th percentile L	38	Entropy of energy R
12	80th percentile R	39	Peak−to−peak amplitude L
13	Interquartile range L	40	Peak−to−peak amplitude R
14	Interquartile range R	41	The number of peaks L
15	Square sum of 20th percentile L	42	The number of peaks R
16	Square sum of 20th percentile R	43	Mean of time between peaks L
17	Square sum of 50th percentile L	44	Mean of time between peaks R
18	Square sum of 50th percentile R	45	Std. of time between peaks L
19	Square sum of 80th percentile L	46	Std. of time between peaks R
20	Square sum of 80th percentile R	47	Prediction ratio L
21	1st bin of binned distribution L	48	Prediction ratio R
22	1st bin of binned distribution R	49	Harmonic ratio L
23	2nd bin of binned distribution L	50	Harmonic ratio R
24	2nd bin of binned distribution R	51	Fundamental frequency L
25	3rd bin of binned distribution L	52	Fundamental frequency R
26	3rd bin of binned distribution R	53	Correlation coefficient of L and R
27	Skenwness L	54	Sigmal magnitude area of L and R

5.2.2. Spectral Features

We extracted statistical features from a spectral frame. A list of the total number of 30 features is given in Table 5.2.

Table 5.2 A list of extracted spectral features

No.	Feature description	No.	Feature description
1	Spectral energy L	16	Spectral spread R
2	Spectral energy R	17	Spectral entropy L
3	Spectral zone 1 of energy L	18	Spectral entropy R
4	Spectral zone 1 of energy R	19	Spectral entropy of energy L
5	Spectral zone 2 of energy L	20	Spectral entropy of energy R
6	Spectral zone 2 of energy R	21	Spectral flux L
7	Spectral zone 3 of energy L	22	Spectral flux R
8	Spectral zone 3 of energy R	23	Spectral rolloff L
9	Spectral zone 4 of energy L	24	Spectral rolloff R
10	Spectral zone 4 of energy R	25	Maximum spectral crest L
11	Spectral zone 5 of energy L	26	Maximum spectral crest R
12	Spectral zone 5 of energy R	27	Spectral skewness L
13	Spectral centroid L	28	Spectral skewness R
14	Spectral centroid R	29	Spectral kurtosis L
15	Spectral spread L	30	Spectral kurtosis R

5.2.3. Feature Vector Generation

An 84-dimentional feature vector was generated by combining the temporal and spectral features above. The generated feature vectors were labeled from the recordings. We repeated this procedures for all frame blocks and generate a series of feature vectors.

Chapter 6

Classification of Featured Activity

6.1. Support Vector Machine (SVM)

This chapter is to select the classifier model of a Support Vector Machine (SVM) [65] by determining parameters which shows the best accuracy from the given problem (*i.e.,* feature vectors). The SVM is a well-known supervised machine learning technique, which shows excellent performance in generalization and robustness using a maximum margin between the classes and a kernel function. We used a grid-search and a cross-validation method to define a penalty parameter C and a kernel parameter γ of the Radial Basis Function (RBF) kernel. A minimum understanding of machine learning techniques and the SVM is required to perform the following procedures. All the procedures in this chapter was implemented using LibSVM [64] software package for MATLAB.

6.2. Design of Classifier Model

6.2.1. Grid−Search

We defined the grid of pairs of (C, γ) for the grid−search with exponentially growing sequences of C (2^{-10}, 2^{-5}, ..., 2^{30}) and γ (2^{-30}, 2^{-25}, ..., 2^{10}) as shown in Fig. 6.3. These sequences were determined heuristically.

6.2.2. Cross−Validation

For each grid of a pair of (C, γ), the 6−fold cross−validation scheme was performed. This scheme divides the entire feature vectors into 6−part subsets, then test one subset from the classifier model trained by the other subsets, and repeat it over all the subsets, one by one. Therefore, every feature vectors can be tested sequentially. Note that each feature to be tested must be scaled, or normalized, from the training subset. For example, the first feature of a feature vector should be scaled linearly to the range of [0, 1] for the all first features in the training feature vectors. This step increases the accuracy of the classification by making the features the equal range and avoiding numerical errors during the calculation. The scale vector obtained from the above was applied to the testing set.

A classification accuracy was calculated on the testing set. The accuracy was calculated from the percentage of feature vectors which are correctly classified. For each grid of a pair of (C, γ), the average accuracy was calculated from all the subsets. The local maximum of the highest accuracy of the grid can be found (see Fig. 6.1). As a result, the precision, recall, and F_1 score of each class of activities were calculated through following equations:

$$\mathrm{Precision} = \frac{\mathrm{TP}}{\mathrm{TP} + \sum \mathrm{FP}} \tag{6.1}$$

$$\mathrm{Recall} = \frac{\mathrm{TP}}{\mathrm{TP} + \sum \mathrm{FN}} \tag{6.2}$$

$$\mathrm{F_1\ score} = 2 \cdot \frac{\mathrm{Precision} \cdot \mathrm{Recall}}{\mathrm{Precision} + \mathrm{Recall}} \tag{6.3}$$

where TP, FP, and FN represent true positives, false positives, and false negatives for each activity, respectively. The confusion matrix of all the activities is given in Table 6.1.

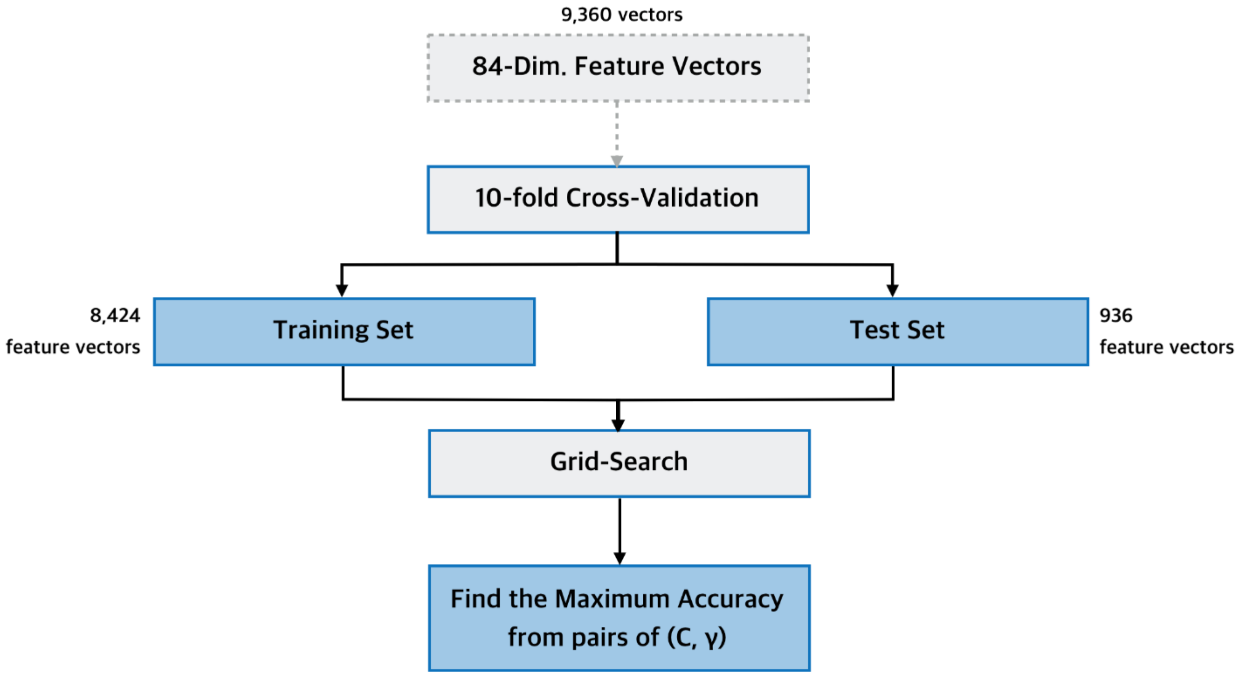

Figure 6.1 Block diagram of classification algorithm

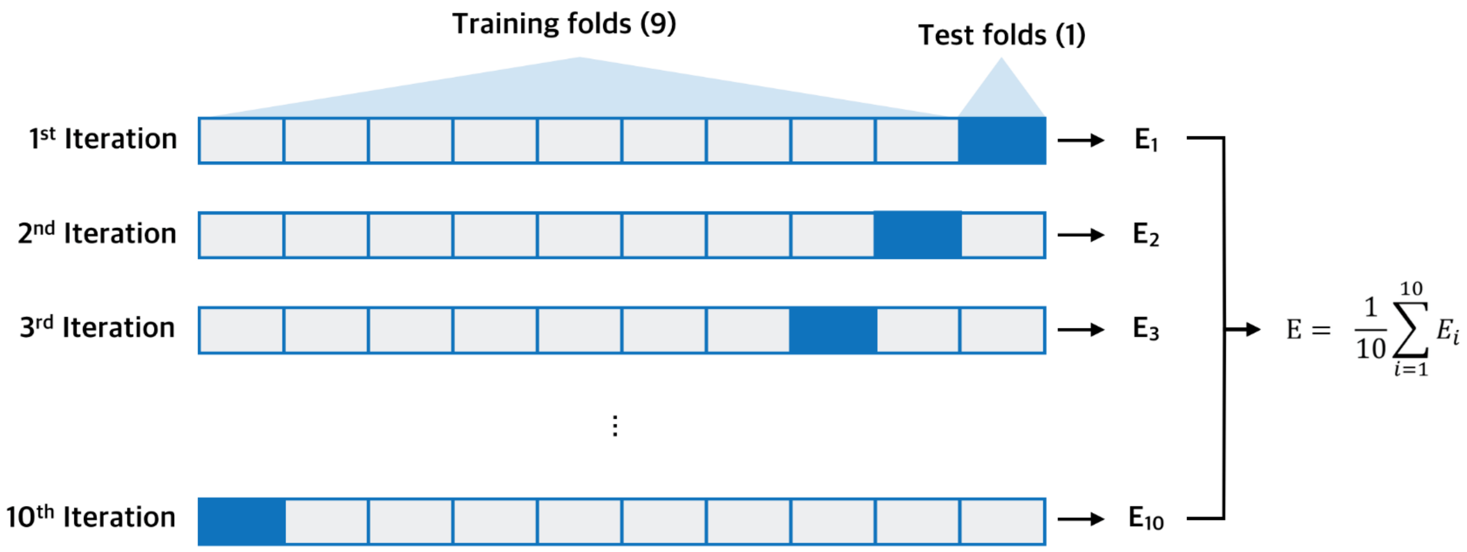

Figure 6.2 Cross−validation scheme

6.3. Classification Result

Table 6.1 shows the representative results of the classification for the entire activity sets. The average F_1 score resulted in 80.5%. If considered as a single score, the performance may seem to be relatively degraded compared to the result of the previous study [60] with the same approach. Significant information, however, can be extracted by comparing the outcomes between each activity. The SR was relatively well distinguished from the SC, CW, and SW, but not from the W and ST. The both chewing activities, the SC and CW, were hard to be distinguished from each other. On the other hand, it can be observed that the both chewing activities can be easily separable from the SR, W, ST, and SW, which represent the other physical activities. In the case of the SW, the wink activity turned out to be misclassified slightly throughout the other activities.

In order to obtain more meaningful results from the above, we grouped and re-defined the activities into new ones. The two chewing activities, SC and CW, were grouped into one activity, and defined as chewing. The SR, W, and ST, which had a large degree of misclassification among themselves, were also grouped into one activity, defined as physical activity. As a result, we obtained new representative results of the classification re−performed through the activities featured as chewing (C), physical activity (PA), and sedentary wink (SW), as shown in Table 6.2. The results showed that the high prediction score with 91.4% of F_1 score.

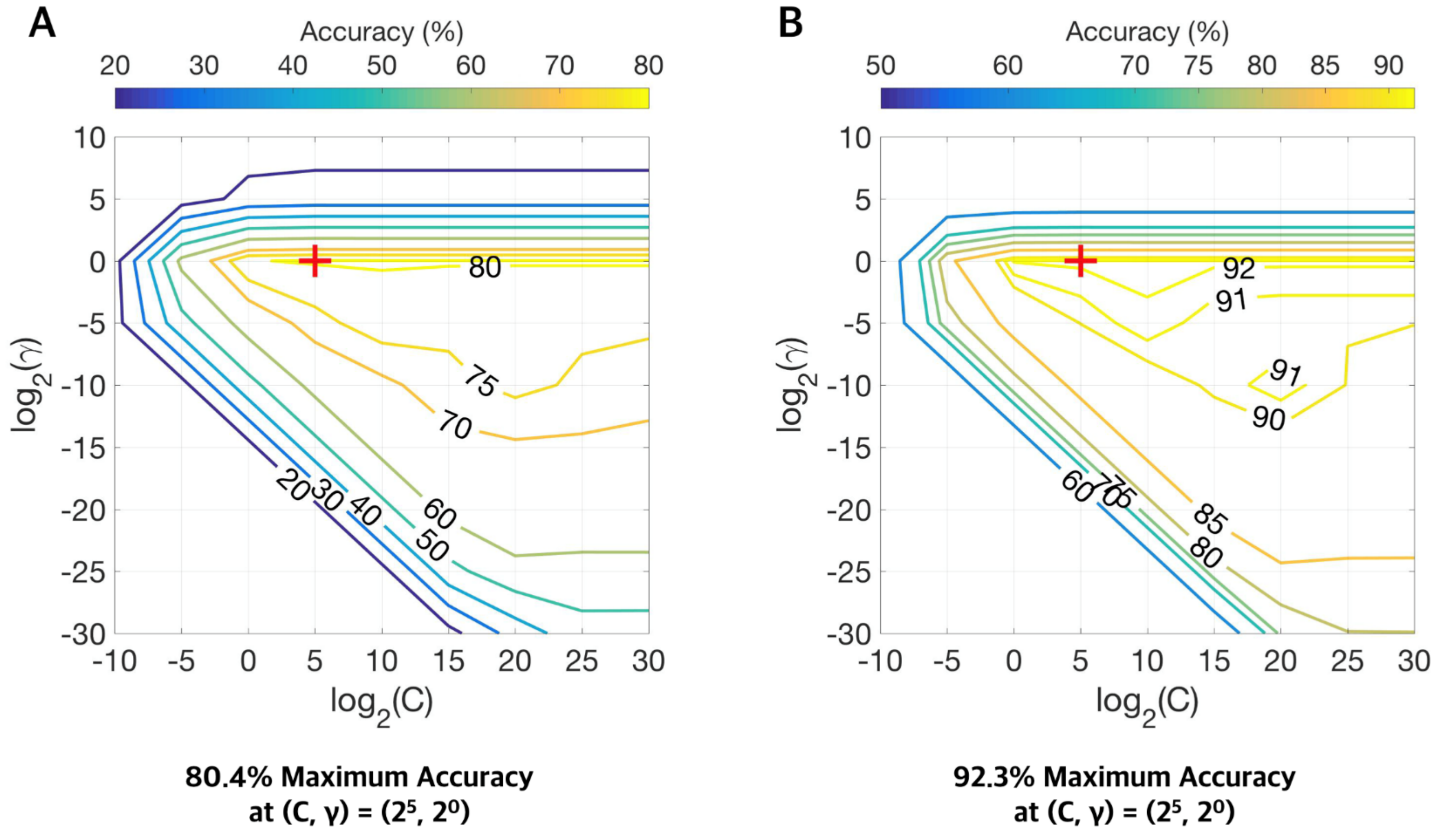

Figure 6.3 Results of grid−search with cross−validation

Table 6.1 Confusion matrix of all the activities when (C, γ) = (2^5, 2^0)

Predicted activity	Actual activity						Total	Precision
	SR	SC	W	CW	ST	SW		
SR	1222	18	79	6	168	75	1568	77.9%
SC	10	1268	17	159	46	15	1515	83.7%
W	55	19	1212	32	144	20	1482	81.8%
CW	3	158	34	1327	28	12	1562	85.0%
ST	192	75	185	19	1117	55	1643	68.0%
SW	78	22	33	17	57	1383	1590	87.0%
Total	1560	1560	1560	1560	1560	1560	9360	
Recall	78.3%	81.3%	77.7%	85.1%	71.6%	88.7%		80.4%
F_1 score	78.1%	82.5%	79.7%	85.0%	69.7%	87.8%		
Average F_1 score		80.5%						

Table 6.2 Confusion matrix of all the re−defined activities when (C, γ) = (2^5, 2^0)

Predicted activity	Actual activity			Total	Precision
	[a]C	[b]PA	[c]SW		
C	2898	162	26	3086	93.9%
PA	201	4404	200	4805	91.7%
SW	21	114	1334	1469	90.8%
Total	3120	4680	1560	9360	
Recall	92.9%	94.1%	85.5%		92.3%
F_1 score	93.4%	92.9%	88.1%		
Average F_1 score		91.4%			

6.4. Performance Improvement

The performance of the classification can be improved by feature selection procedures. The feature selection is the process of selecting a subset of relevant features which simplify the given problem, reduce training times, avoid the curse of dimensionality, and enhance generalization by reducing overfitting [66]. This study used the forward feature selection (FFS) procedures, which is depicted in Fig. 6.4.

The performance of the all activities improved from 80.4% to 85.8% by verifying the features and eliminating redundant features. A total of 29 features were selected before the performance was saturated and diminished. The performance of the re-defined activities was improved from 92.3% to 93.7% as well. A total of 26 features were selected as shown in Fig. 6.7 and Table 6.4.

Figure 6.6 shows the scatter plot of the first two selected features of the all activities. Some notable observations were found: two chewing activities have small spectral spread and skewness; rest, talking, walking have large spectral spread; rest, talking, walking have small skewness; wink has large skewness; and wink was spread on spectral spread. Figure 6.8 shows the scatter plot of the first two selected features of the re-defined activities. Some notable observations were found as well: chewing has large signal magnitude area (SMA); chewing has small SMA; wink has large skewness; wink has small SMA; and physical activities have small SMA and skewness.

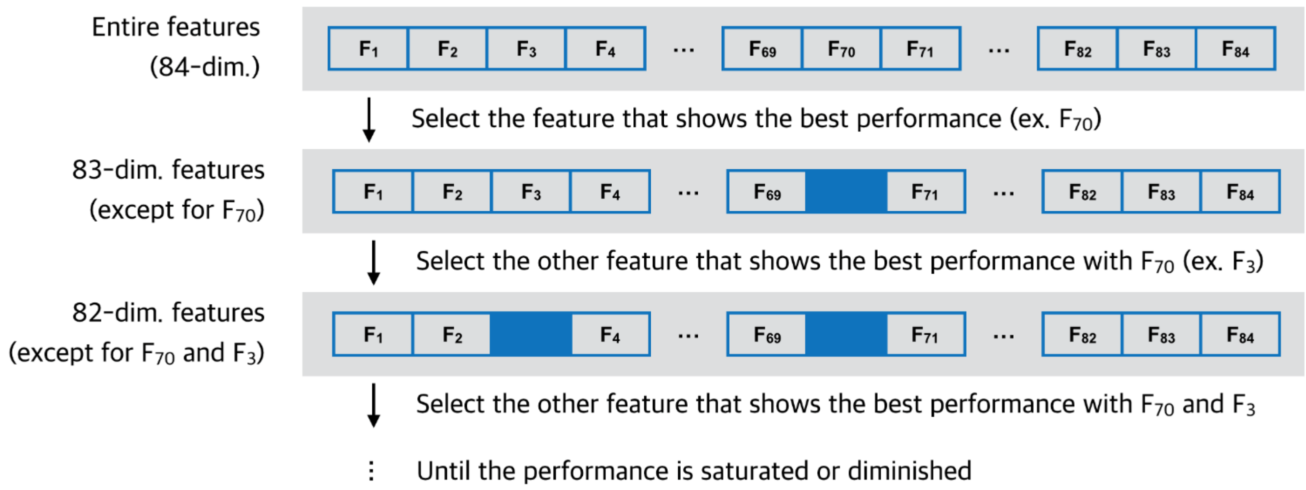

Figure 6.4 Algorithm of forward feature selection procedure

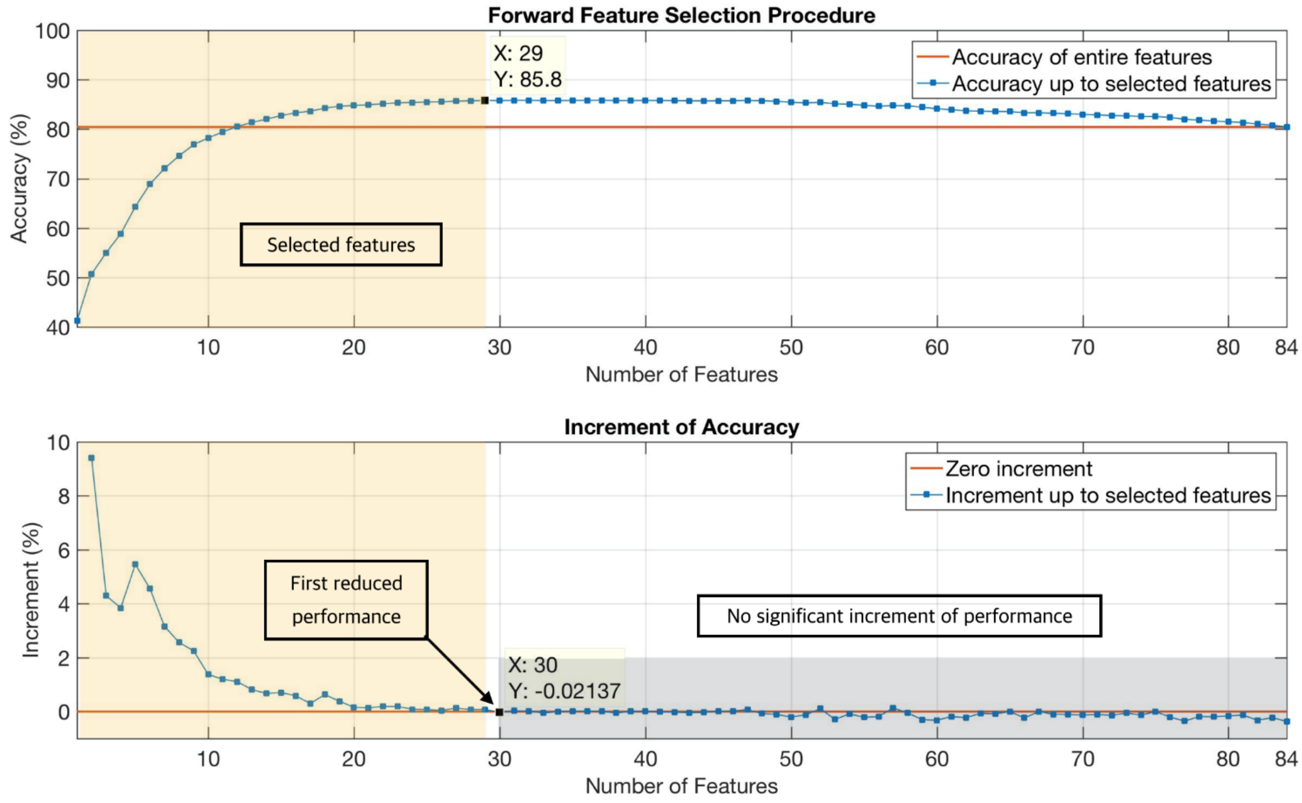

Figure 6.5 Forward feature selection procedure for the entire activities

Table 6.3 List of selected features for the entire activities

	Selected Feature	Accuracy (%)
1	Spectral spread (R)	41.3
2	Skenwness (R)	50.7
3	Log signal energy (R)	55.0
4	20^{th} percentile (L)	58.9
5	80^{th} percentile (R)	64.3
6	Spectral spread (L)	68.9
7	Correlation coefficient	72.0
8	Log signal energy (R)	74.6
9	Spectral centroid (R)	76.9
10	Peak-to-peak amplitude (L)	78.2
11	Spectral centroid (L)	79.4
12	20^{th} percentile (R)	80.5
13	Peak-to-peak amplitude (R)	81.4
14	80^{th} percentile (L)	82.0
15	Zero crossing rate (R)	82.7
16	Entropy of energy (R)	83.3
17	50^{th} percentile (R)	83.6
18	50^{th} percentile (L)	84.3
19	Harmonic ratio (R)	84.6
20	Standard deviation (L)	84.8
21	Spectral energy (R)	84.9
22	Skenwness (L)	85.1
23	5^{th} Sub-band spectral energy (R)	85.3
24	Standard deviation (R)	85.4
25	Spectral rolloff (L)	85.5
26	Entropy of energy (L)	85.5
27	Spectral entropy (L)	85.7
28	Spectral energy (L)	85.7
29	Coefficient of vacation (L)	85.8

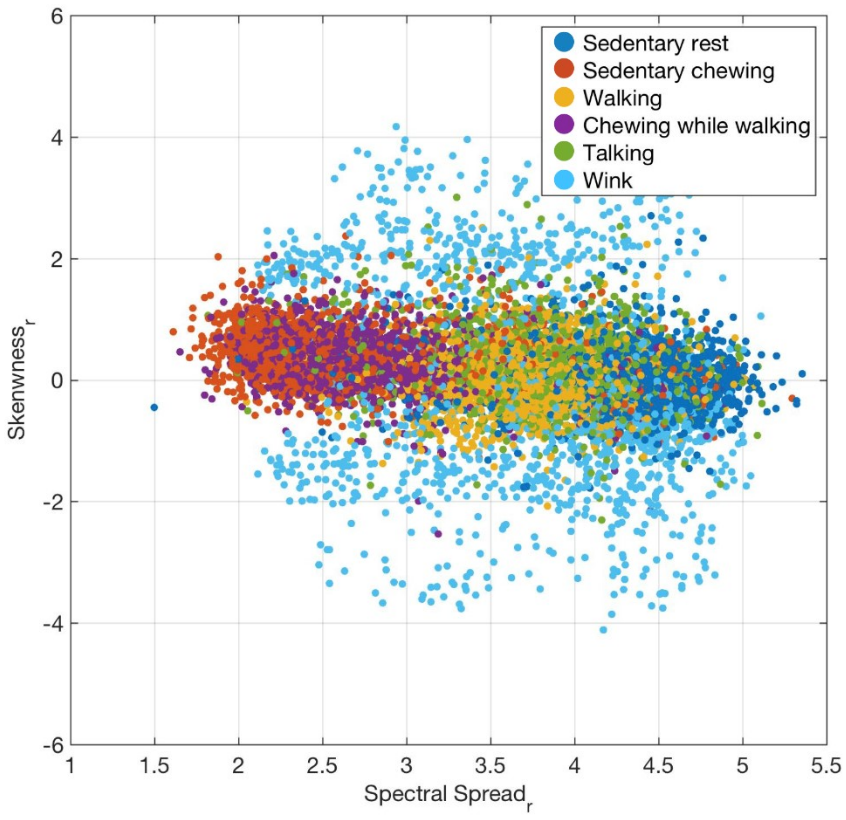

Figure 6.6 Scatter plot of 1st and 2nd selected features for the entire activities

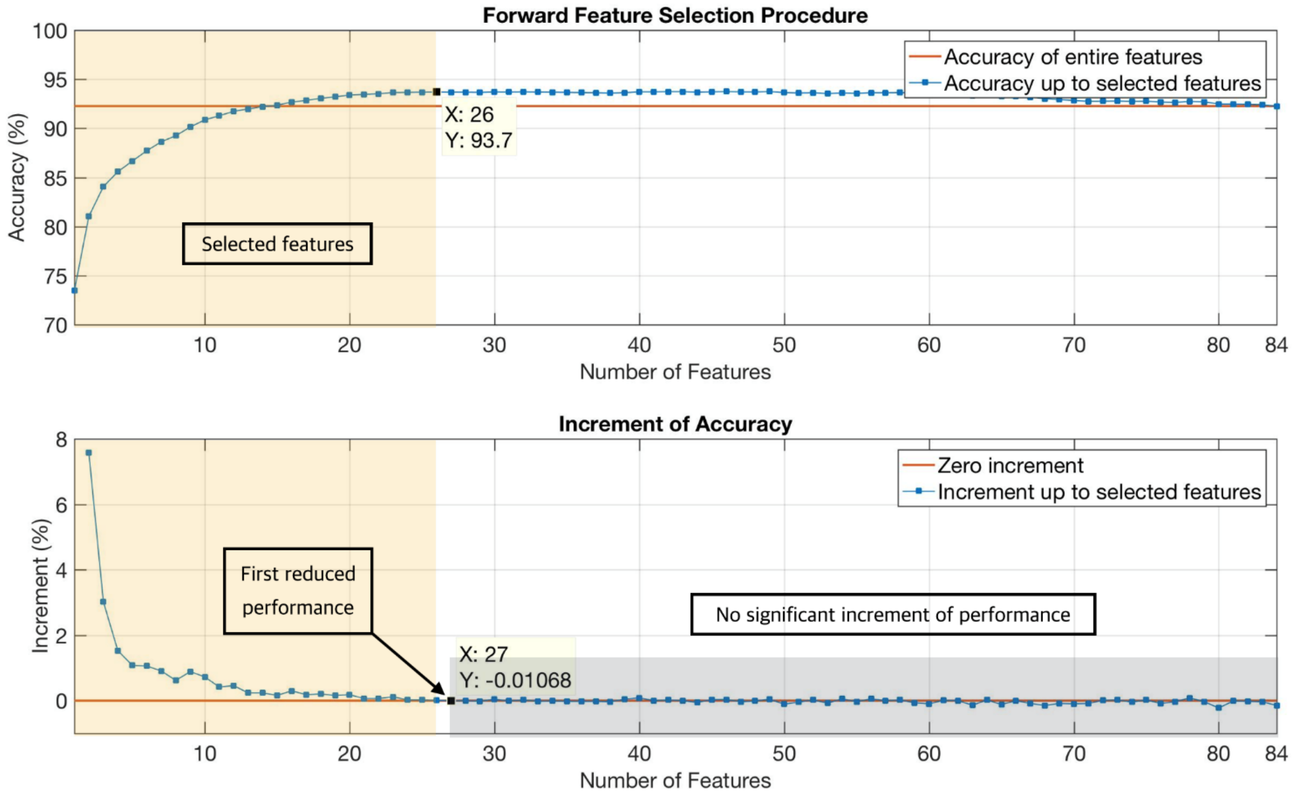

Figure 6.7 Forward feature selection procedure for the re−defined activities

Table 6.4 List of selected features for the re-defined activities

	Selected Feature	Accuracy (%)
1	Signal magnitude area	73.5
2	Skenwness (R)	81.0
3	Correlation coefficient	84.1
4	Harmonic ratio (L)	85.6
5	20^{th} percentile (L)	86.7
6	80^{th} percentile (R)	87.7
7	Spectral crest (L)	88.6
8	Entropy of energy (R)	89.3
9	Log signal energy (L)	90.1
10	Spectral spread (L)	90.9
11	Spectral Skenwness (R)	91.3
12	Peak-to-peak amplitude (L)	91.7
13	Standard deviation (R)	92.0
14	50^{th} percentile (L)	92.2
15	Fundamental frequency (R)	92.4
16	Skewness (L)	92.7
17	20^{th} percentile (R)	92.9
18	The number of peaks (L)	93.1
19	Log signal energy (R)	93.2
20	80^{th} percentile (L)	93.4
21	Spectral crest (R)	93.5
22	50^{th} percentile (R)	93.5
23	Spectral entropy of energy (L)	93.6
24	Entropy of energy (L)	93.7
25	Standard deviation (L)	93.7
26	Square sum up to 80^{th} percentile (R)	93.7

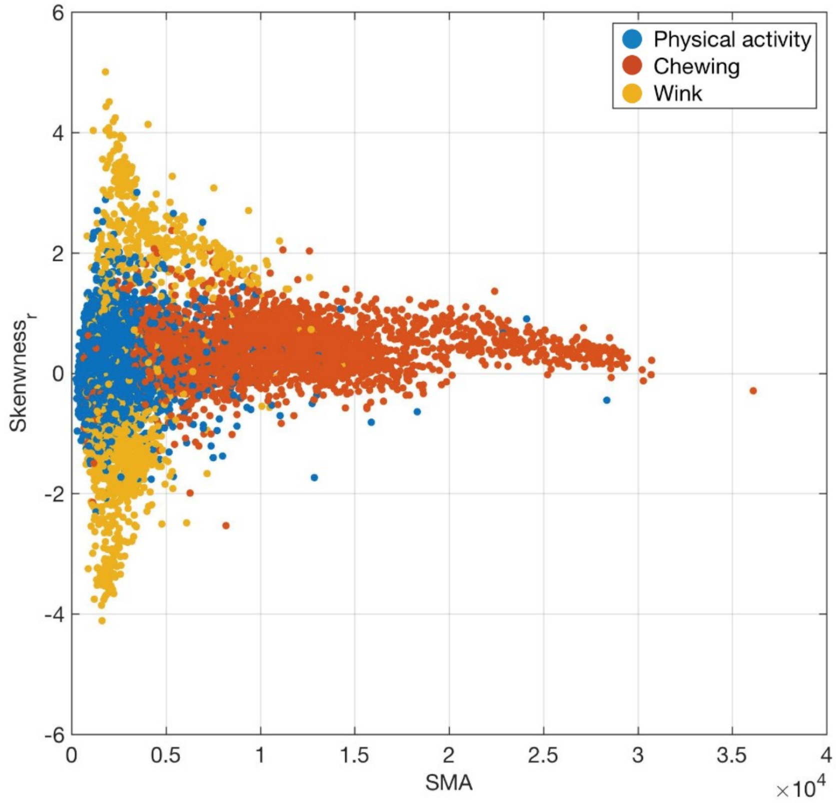

Figure 6.8 Scatter plot of 1st and 2nd selected features for the re−defined activities

6.5. Discussion

To obtain the reliable data reflecting different head sizes and shapes for each subject, two versions of the glasses were provided by varying the length of the head piece and temples. In addition, utilizing the support volts to fine−tune the wearability, we could adjust the tightness of the glasses. Thus, the data collected through the various glasses, subjects, and wearing conditions could reflect intra− and inter−individual variability and different form factors.

According to an earlier study of chewing frequency, the chewing activity is mainly ranged from the 0.94 Hz (5th percentile) to the 2.17 Hz (95th percentile) [61]. Thus, this study set the frame size to 2 seconds so that a frame contains multiple chewing activities. This frame size is also suitable for containing the one or more walking cycles generally ranged from 1.4 Hz to 2.5 Hz [67]. We conducted the walking activity at a speed of 4.5 km/h on a treadmill, because the normal walking speed varies from 3.3 km/h to 6.5 km/h [67, 68]. The hop size in Fig. 4.1 was determined from that we had recorded the wink data at 1−second intervals by informing the subjects of the exact performing time from sound. We also filtered the data with the cutoff frequency of 10 Hz, because we found that the signals over 10 Hz had no significant information on chewing detection from our previous study [60].

From the results of the Table 6.1, we can discuss in-depth details of the classification. First, the two chewing activities, SC and CW, were clearly distinguished from the other activities. Among them, the distinction from the walking activity suggests a possibility that the food intake activity, which is the main purpose of this study, can be easily separable from the active physical activity, such as walking, using our system. As shown in Fig. 4.1, it can be verified that the chewing and wink signals, activated from the temporals muscle activity, were significantly different from those not. On the other hand, the distinction between the two chewing activities showed relatively high misclassifications. They played a dominant role in lowering the both precision and recall of the chewing activities.

In terms of chewing detection, the SR, W and ST can be regarded as unintended noise in daily life. The wink activity, on the other hand, can be considered as meaningful measurement, because it is also activated from the temporalis muscle activity as well. Based on the above, the two chewing activities were bounded into a chewing activity (C), and the other activities except for the wink were grouped into a physical activity (PA). Table 6.2 shows the classification results on these activities: chewing (C), physical activity (PA), and sedentary wink (SW). We can find more remarkable results from it. It connotes the information about whether the system is robust on detecting food intake without being affected by other physical activities. Furthermore, it also indicates whether it is possible to distinguish food intake from other face activity such as wink. The results show that the chewing activity can be well distinguished from the other activities by a high F1 score of 93.4%. In the case of wink, the recall (85.5%) was slightly lower than that of the other activities. This means that the quality of the collected data of wink was likely to be low, as the users had to wink at exact time in 3−second intervals. In fact, it was observed that the users missed the wink or the glasses flowed down occasionally during the user study.

Because the system has two load cells on both sides, it can be possible to distinguish the left and right events of the chewing and wink, as proved in our previous study [60]. Unlike the previous one, the aim of this study was focused on showing the ability that the system could effectively separate food intake from the physical activities. If the data will be sufficiently accumulated through the user study, the further research on the left and right classification can be conducted, utilizing the correlation features included in the feature vector. On the other hand, it is hard to distinguish between the sedentary activity and walking with the system. If possible, the detailed classification of the food intake like eating while sitting, and eating on the move will be available with a high accuracy. This can be implemented through a sensor fusion technique by adding an inertial measurement unit (IMU) to the system [7] . If so, the system can track the energy expenditure and the energy intake simultaneously. There have been previous approaches on energy estimation [69], and this concern will be the main goal of the dietary monitoring. We believe that our approach provided the practical and potential ways to the detection of food intake and physical activities.

Chapter 7

Conclusions

In this study, we first proposed the design and manufacturing process of the glasses that sense the patterns of the food intake and physical activities. As this study mainly focused on the data analysis to distinguish the food intake from the other physical activities such as walking and wink, the sensor and data acquisition system needed to be implemented to provide mobility. Thus, the system included the sensors, the MCU with wireless communication capability, and the battery. The proposed protocol provided a novel and practical way to measure the temporalis muscles activity due to the food intake and wink in a non−contact manner. It is significant in that it provided the tools and methodologies that can easily detect the food intake in daily life without any cumbersome equipment.

We are continuing this research in order to enhance practical usability in daily life. There are more dynamic physical behaviors, such as head shaking, and running, which can affect the measured force signal from the hinge. In order to examine the effects of those behaviors, an extended user study will be conducted. This can be achieved by adding a MEMS accelerometer sensor to the device to cancel the force due to the body movement. From this sensor fusion technique, the monitoring of both the energy intake and energy expenditure can be tracked in daily life.

Our approach has another strength on the sensing methodology because it utilizes the indirect contact with skin. If the sensor is attached or contact with the epidermis, it is prone to be damaged or removed from the body. We expect that the non-intrusive and contactless sensors in the form of the wearable glasses can achieve a robust monitoring of ingestive behaviors with a higher accuracy through these investigations.

Here, we also want to discuss potential of our device as glassware wearable capable of recognizing facial patterns, such as [70], in a hands-free controller format. Recently, Google glass-based wearable device has been developed to control voice recognition commands into their biomedical applications [71]. Their approach seems very creative and helpful for people who may require hands-free behaviors and motions in a controlled manner. In this sense, this study can give us the potential to supplement the lack of input methods in AR or VR applications without disrupting other activities. Furthermore, through applying this approach to a sensor-integrated hair band, it can be potentially used for the medical monitoring of the sleep bruxism [72-76] or temporomandibular dysfunction. We further believe that our approach can be an innovative wearable device for monitoring and controlling a set of facial behaviors such as chewing and talking in a daily lifecare format.

	Unique measurement	Unique sensor	Unique utilization	Unique amplification	Indirect contact	Monitoring with physical activity
Ref.	**Approach(es)**	**Sensor(s)**	**Sensing location**	**Amplification Type**	**Contact type**	**Classes**
Ishimaru, et al., 2014	Electrometric, Inertial	Electrooculography (EOG), Accelerometer	Nose pad, Bridge	Electrical	Direct	Eating, Reading, Typing, Talking
Merte, et al, 2015	Inertial	Accelerometer	Temple	Electrical	Indirect	Chewing, Non-chewing, Walking
Farooq, et al, 2016	Morphological	Piezoelectric strain sensor	Epidermis	Electrical	Direct	Chewing, Non-chewing
Zhang, et al., 2016	Electrometric	Electromyography (EMG)	Nose pad, Temple	Electrical	Direct	Toast, Carrot, Banana, Jelly baby, Biscuit
Farooq, et al., 2016	Inertial, Morphological	Accelerometer, Piezoelectric strain sensor	Temple, Epidermis	Electrical	Direct	Eating+Sitting, Eating+Walking, Sedentary, Walking
Huang, et al., 2017	Electrometric	EMG	Temple	Electrical	Direct	Apple, Banana, Blue berries, Bread, Crackers
Zhang, et al., 2017	Electrometric	EMG	Temple	Electrical	Direct	Carrot, Cucumber, Banana
Chung, et al., 2017	**Force**	**Load cells**	**Hinge**	**Mechanical, Electrical**	**Indirect**	**Left and right chewing, Left and right wink, Talking, Walking**

Figure 7.1 Uniqueness and novelty of the presented solution in this study

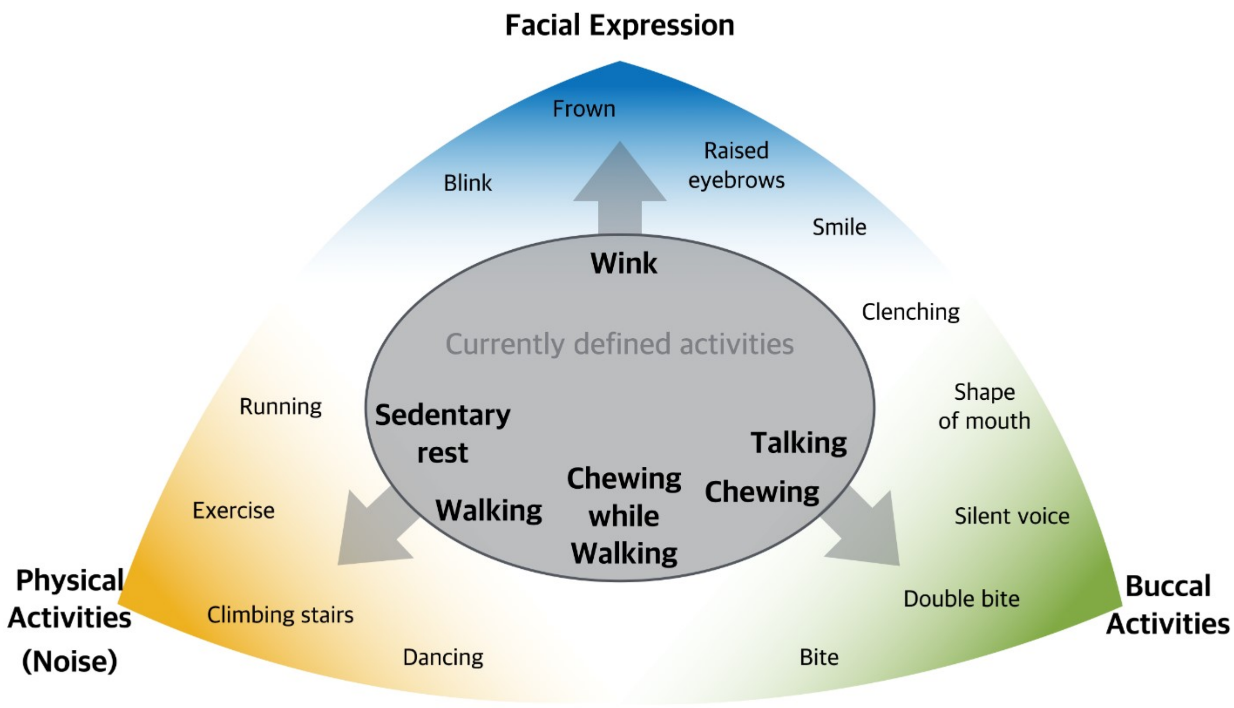

Figure 7.2 Potentials of the system through the activity expansion

Bibliography

[1] A. P. Usher, "A History of Mechanical Inventions (New York, 1929)," *UsherA History of Mechanical Inventions1929*.

[2] S. Standring, *Gray's anatomy: the anatomical basis of clinical practice*. Elsevier Health Sciences, 2015.

[3] R. I. Ramos-Garcia and A. W. Hoover, "A study of temporal action sequencing during consumption of a meal," in *Proceedings of the International Conference on Bioinformatics, Computational Biology and Biomedical Informatics*, 2013, p. 68: ACM.

[4] P. J. S. A. Strini, P. J. S. A. Strini, T. de Souza Barbosa, and M. B. D. Gavião, "Assessment of thickness and function of masticatory and cervical muscles in adults with and without temporomandibular disorders," *Archives of oral biology,* vol. 58, no. 9, pp. 1100-1108, 2013.

[5] G. Mertes, H. Hallez, T. Croonenborghs, and B. Vanrumste, "Detection of chewing motion using a glasses mounted accelerometer towards monitoring of food intake events in the elderly," in *International Conference on Biomedical and Health Informatics*, 2015, pp. 1-5.

[6] S. Ishimaru, K. Kunze, K. Tanaka, Y. Uema, K. Kise, and M. Inami, "Smart eyewear for interaction and activity recognition," in *Proceedings of the 33rd Annual ACM Conference Extended Abstracts on Human Factors in Computing Systems*, 2015, pp. 307-310: ACM.

[7] M. Farooq and E. Sazonov, "A novel wearable device for food intake and physical activity recognition," *Sensors,* vol. 16, no. 7, p. 1067,

2016.

[8] R. Zhang, S. Bernhart, and O. Amft, "Diet eyeglasses: Recognising food chewing using EMG and smart eyeglasses," in *Wearable and Implantable Body Sensor Networks (BSN), 2016 IEEE 13th International Conference on*, 2016, pp. 7-12: IEEE.

[9] A. Sharma and R. Padwal, "Obesity is a sign–over-eating is a symptom: an aetiological framework for the assessment and management of obesity," *Obesity reviews,* vol. 11, no. 5, pp. 362-370, 2010.

[10] A. M. Sharma and R. Padwal, "Obesity is a sign–over-eating is a symptom: an aetiological framework for the assessment and management of obesity," *Obesity reviews,* vol. 11, no. 5, pp. 362-370, 2010.

[11] F. X. Pi-Sunyer *et al.*, "Clinical guidelines on the identification, evaluation, and treatment of overweight and obesity in adults," *American Journal of Clinical Nutrition,* vol. 68, no. 4, pp. 899-917, 1998.

[12] P. McCrory, B. Strauss, and M. L. Wahlqvist, "Energy balance, food intake and obesity," *Exercise and obesity London,* 1994.

[13] S. Mendis, "Global status report on noncommunicable diseases 2014," World Health Organization2014.

[14] F. X. Pi-Sunyer *et al.*, "Clinical guidelines on the identification, evaluation, and treatment of overweight and obesity in adults: Executive summary," *American Journal of Clinical Nutrition,* vol. 68, no. 4, pp. 899-917, 1998.

[15] P. T. James, "Obesity: the worldwide epidemic," *Clinics in dermatology,* vol. 22, no. 4, pp. 276-280, 2004.

[16] F. Albinali, S. Intille, W. Haskell, and M. Rosenberger, "Using wearable activity type detection to improve physical activity energy expenditure estimation," in *Proceedings of the 12th ACM international conference on Ubiquitous computing*, 2010, pp. 311-320: ACM.

[17] A. Bonomi and K. Westerterp, "Advances in physical activity monitoring and lifestyle interventions in obesity: a review," *International journal of obesity,* vol. 36, no. 2, pp. 167-177, 2012.

[18] S. Jung, J. Lee, T. Hyeon, M. Lee, and D. H. Kim, "Fabric-Based Integrated Energy Devices for Wearable Activity Monitors," *Advanced Materials,* vol. 26, no. 36, pp. 6329-6334, 2014.

[19] S. Jung *et al.*, "Wearable fall detector using integrated sensors and energy devices," *Scientific reports,* vol. 5, 2015.

[20] R. J. McNamara *et al.*, "Measurement of daily physical activity using the SenseWear Armband: Compliance, comfort, adverse side effects and usability," *Chronic respiratory disease,* vol. 13, no. 2, pp. 144-154, 2016.

[21] S. C. Mukhopadhyay, "Wearable sensors for human activity monitoring: A review," *IEEE sensors journal,* vol. 15, no. 3, pp. 1321-1330, 2015.

[22] G. D. Fulk and E. Sazonov, "Using sensors to measure activity in people with stroke," *Topics in stroke rehabilitation,* vol. 18, no. 6, pp. 746-757, 2011.

[23] T. Prioleau, E. Moore, and M. Ghovanloo, "Unobtrusive and Wearable

Systems for Automatic Dietary Monitoring," *IEEE Transactions on Biomedical Engineering,* 2017.

[24] T. Vu, F. Lin, N. Alshurafa, and W. Xu, "Wearable Food Intake Monitoring Technologies: A Comprehensive Review," *Computers,* vol. 6, no. 1, p. 4, 2017.

[25] D. Wen, X. Zhang, X. Liu, and J. Lei, "Evaluating the Consistency of Current Mainstream Wearable Devices in Health Monitoring: A Comparison Under Free-Living Conditions," *Journal of medical Internet research,* vol. 19, no. 3, 2017.

[26] H. Kalantarian, N. Alshurafa, and M. Sarrafzadeh, "a Survey of Diet Monitoring technology," *IEEE Pervasive Computing,* vol. 16, no. 1, pp. 57-65, 2017.

[27] P. Pouladzadeh, S. Shirmohammadi, and A. Yassine, "You are what you eat: So measure what you eat!," *IEEE Instrumentation & Measurement Magazine,* vol. 19, no. 1, pp. 9-15, 2016.

[28] O. Makeyev, P. Lopez-Meyer, S. Schuckers, W. Besio, and E. Sazonov, "Automatic food intake detection based on swallowing sounds," *Biomedical signal processing and control,* vol. 7, no. 6, pp. 649-656, 2012.

[29] S. Passler and W.-J. Fischer, "Food intake monitoring: Automated chew event detection in chewing sounds," *Biomedical and Health Informatics, IEEE Journal of,* vol. 18, no. 1, pp. 278-289, 2014.

[30] S. Päßler and W. Fischer, "Food intake activity detection using an artificial neural network," *Biomed Tech (Berl),* 2012.

[31] S. Passler and W.-J. Fischer, "Food intake monitoring: Automated chew event detection in chewing sounds," *IEEE journal of biomedical and health informatics,* vol. 18, no. 1, pp. 278-289, 2014.

[32] T. Olubanjo and M. Ghovanloo, "Real-time swallowing detection based on tracheal acoustics," in *Acoustics, Speech and Signal Processing (ICASSP), 2014 IEEE International Conference on*, 2014, pp. 4384-4388: IEEE.

[33] W. P. Walker and D. K. Bhatia, "Automated ingestion detection for a health monitoring system," *IEEE journal of biomedical and health informatics,* vol. 18, no. 2, pp. 682-692, 2014.

[34] E. S. Sazonov and J. M. Fontana, "A sensor system for automatic detection of food intake through non-invasive monitoring of chewing," *Sensors Journal, IEEE,* vol. 12, no. 5, pp. 1340-1348, 2012.

[35] H. Kalantarian, N. Alshurafa, T. Le, and M. Sarrafzadeh, "Monitoring eating habits using a piezoelectric sensor-based necklace," *Computers in biology and medicine,* vol. 58, pp. 46-55, 2015.

[36] M. Farooq and E. Sazonov, "Linear regression models for chew count estimation from piezoelectric sensor signals," in *Sensing Technology (ICST), 2016 10th International Conference on*, 2016, pp. 1-5: IEEE.

[37] N. Alshurafa *et al.*, "Recognition of nutrition intake using time-frequency decomposition in a wearable necklace using a piezoelectric sensor," *IEEE sensors journal,* vol. 15, no. 7, pp. 3909-3916, 2015.

[38] N. Alshurafa, H. Kalantarian, M. Pourhomayoun, S. Sarin, J. J. Liu, and M. Sarrafzadeh, "Non-invasive monitoring of eating behavior using spectrogram analysis in a wearable necklace," in *Healthcare*

Innovation Conference (HIC), 2014 IEEE, 2014, pp. 71-74: IEEE.

[39] H. Kalantarian, N. Alshurafa, and M. Sarrafzadeh, "A wearable nutrition monitoring system," in *Wearable and Implantable Body Sensor Networks (BSN), 2014 11th International Conference on*, 2014, pp. 75-80: IEEE.

[40] A. Bedri, A. Verlekar, E. Thomaz, V. Avva, and T. Starner, "A wearable system for detecting eating activities with proximity sensors in the outer ear," in *Proceedings of the 2015 ACM International Symposium on Wearable Computers*, 2015, pp. 91-92: ACM.

[41] Y. Bai, W. Jia, Z.-H. Mao, and M. Sun, "Automatic eating detection using a proximity sensor," in *Bioengineering Conference (NEBEC), 2014 40th Annual Northeast*, 2014, pp. 1-2: IEEE.

[42] A. Kadomura, C.-Y. Li, Y.-C. Chen, K. Tsukada, I. Siio, and H.-h. Chu, "Sensing fork: eating behavior detection utensil and mobile persuasive game," in *CHI'13 Extended Abstracts on Human Factors in Computing Systems*, 2013, pp. 1551-1556: ACM.

[43] J. M. Fontana, M. Farooq, and E. Sazonov, "Automatic ingestion monitor: a novel wearable device for monitoring of ingestive behavior," *Biomedical Engineering, IEEE Transactions on,* vol. 61, no. 6, pp. 1772-1779, 2014.

[44] J. M. Fontana, M. Farooq, and E. Sazonov, "Automatic ingestion monitor: A novel wearable device for monitoring of ingestive behavior," *IEEE Transactions on Biomedical Engineering,* vol. 61, no. 6, pp. 1772-1779, 2014.

[45] Y. Shen, J. Salley, E. Muth, and A. Hoover, "Assessing the Accuracy

of a Wrist Motion Tracking Method for Counting Bites across Demographic and Food Variables," *IEEE Journal of Biomedical and Health Informatics,* 2016.

[46] S. Wang, G. Zhou, L. Hu, Z. Chen, and Y. Chen, "CARE: Chewing activity recognition using noninvasive single axis accelerometer," in *Adjunct Proceedings of the 2015 ACM International Joint Conference on Pervasive and Ubiquitous Computing and Proceedings of the 2015 ACM International Symposium on Wearable Computers*, 2015, pp. 109-112: ACM.

[47] E. Thomaz, I. Essa, and G. D. Abowd, "A practical approach for recognizing eating moments with wrist-mounted inertial sensing," in *Proceedings of the 2015 ACM International Joint Conference on Pervasive and Ubiquitous Computing*, 2015, pp. 1029-1040: ACM.

[48] R. I. Ramos-Garcia, E. R. Muth, J. N. Gowdy, and A. W. Hoover, "Improving the recognition of eating gestures using intergesture sequential dependencies," *IEEE journal of biomedical and health informatics,* vol. 19, no. 3, pp. 825-831, 2015.

[49] Y. Dong, J. Scisco, M. Wilson, E. Muth, and A. Hoover, "Detecting periods of eating during free-living by tracking wrist motion," *IEEE journal of biomedical and health informatics,* vol. 18, no. 4, pp. 1253-1260, 2014.

[50] M. Farooq and E. Sazonov, "Feature Extraction Using Deep Learning for Food Type Recognition," in *International Conference on Bioinformatics and Biomedical Engineering*, 2017, pp. 464-472: Springer.

[51] F. Kong, H. He, H. A. Raynor, and J. Tan, "DietCam: Multi-view regular shape food recognition with a camera phone," *Pervasive and Mobile Computing,* vol. 19, pp. 108-121, 2015.

[52] M. Farooq, J. M. Fontana, and E. Sazonov, "A novel approach for food intake detection using electroglottography," *Physiological measurement,* vol. 35, no. 5, p. 739, 2014.

[53] A. Grigoriadis, R. S. Johansson, and M. Trulsson, "Temporal profile and amplitude of human masseter muscle activity is adapted to food properties during individual chewing cycles," *Journal of oral rehabilitation,* vol. 41, no. 5, pp. 367-373, 2014.

[54] R. Zhang and O. Amft, "Monitoring chewing and eating in free-living using smart eyeglasses," *IEEE Journal of Biomedical and Health Informatics,* 2017.

[55] S. Ishimaru, K. Kunze, Y. Uema, K. Kise, M. Inami, and K. Tanaka, "Smarter eyewear: using commercial EOG glasses for activity recognition," in *Proceedings of the 2014 ACM International Joint Conference on Pervasive and Ubiquitous Computing: Adjunct Publication*, 2014, pp. 239-242: ACM.

[56] B. Zhou *et al.*, "Smart table surface: A novel approach to pervasive dining monitoring," in *Pervasive Computing and Communications (PerCom), 2015 IEEE International Conference on*, 2015, pp. 155-162: IEEE.

[57] R. Zhang and O. Amft, "Bite glasses: measuring chewing using emg and bone vibration in smart eyeglasses," in *Proceedings of the 2016 ACM International Symposium on Wearable Computers*, 2016, pp. 50-

52: ACM.

[58] M. Farooq and E. Sazonov, "Segmentation and Characterization of Chewing Bouts by Monitoring Temporalis Muscle Using Smart Glasses with Piezoelectric Sensor," *IEEE Journal of Biomedical and Health Informatics,* 2016.

[59] Q. Huang, W. Wang, and Q. Zhang, "Your Glasses Know Your Diet: Dietary Monitoring using Electromyography Sensors," *IEEE Internet of Things Journal,* 2017.

[60] J. Chung, J. Chung, W. Oh, Y. Yoo, W. G. Lee, and H. Bang, "A glasses-type wearable device for monitoring the patterns of food intake and facial activity," *Scientific Reports,* vol. 7, p. 41690, 2017.

[61] J. Po, J. Kieser, L. Gallo, A. Tésenyi, P. Herbison, and M. Farella, "Time-frequency analysis of chewing activity in the natural environment," *Journal of dental research,* vol. 90, no. 10, pp. 1206-1210, 2011.

[62] T. Giannakopoulos and A. Pikrakis, *Introduction to Audio Analysis: A MATLAB® Approach*. Academic Press, 2014.

[63] N. Cristianini and J. Shawe-Taylor, *An introduction to support vector machines and other kernel-based learning methods*. Cambridge university press, 2000.

[64] C.-C. Chang and C.-J. Lin, "LIBSVM: a library for support vector machines," *ACM Transactions on Intelligent Systems and Technology (TIST),* vol. 2, no. 3, p. 27, 2011.

[65] N. Cristianini and J. Shawe-Taylor, "An introduction to support vector

machines," ed: Cambridge University Press Cambridge, 2000.

[66] M. L. Bermingham *et al.*, "Application of high-dimensional feature selection: evaluation for genomic prediction in man," *Scientific reports,* vol. 5, 2015.

[67] T. Ji, "Frequency and velocity of people walking," *Structural Engineer,* vol. 84, no. 3, pp. 36-40, 2005.

[68] R. Knoblauch, M. Pietrucha, and M. Nitzburg, "Field studies of pedestrian walking speed and start-up time," *Transportation Research Record: Journal of the Transportation Research Board,* no. 1538, pp. 27-38, 1996.

[69] J. M. Fontana *et al.*, "Energy intake estimation from counts of chews and swallows," *Appetite,* vol. 85, pp. 14-21, 2015.

[70] D. J. Matthies, B. A. Strecker, and B. Urban, "EarFieldSensing: A Novel In-Ear Electric Field Sensing to Enrich Wearable Gesture Input through Facial Expressions," in *Proceedings of the 2017 CHI Conference on Human Factors in Computing Systems*, 2017, pp. 1911-1922: ACM.

[71] Y. S. Zhang *et al.*, "Google Glass-Directed Monitoring and Control of Microfluidic Biosensors and Actuators," *Scientific reports,* vol. 6, 2016.

[72] P. McAuliffe, J. H. Kim, D. Diamond, K. Lau, and B. O'connell, "A sleep bruxism detection system based on sensors in a splint-pilot clinical data," *Journal of oral rehabilitation,* vol. 42, no. 1, pp. 34-39, 2015.

[73] A. Deregibus, T. Castroflorio, A. Bargellini, and C. Debernardi,

"Reliability of a portable device for the detection of sleep bruxism," *Clinical oral investigations,* vol. 18, no. 8, pp. 2037-2043, 2014.

[74] T. Castroflorio, A. Deregibus, A. Bargellini, C. Debernardi, and D. Manfredini, "Detection of sleep bruxism: comparison between an electromyographic and electrocardiographic portable holter and polysomnography," *Journal of oral rehabilitation,* vol. 41, no. 3, pp. 163-169, 2014.

[75] N. Jirakittayakorn and Y. Wongsawat, "An EMG instrument designed for bruxism detection on masseter muscle," in *Biomedical Engineering International Conference (BMEiCON), 2014 7th*, 2014, pp. 1-5: IEEE.

[76] T. Castroflorio, L. Mesin, G. M. Tartaglia, C. Sforza, and D. Farina, "Use of electromyographic and electrocardiographic signals to detect sleep bruxism episodes in a natural environment," *IEEE journal of biomedical and health informatics,* vol. 17, no. 6, pp. 994-1001, 2013.

초 록

최근의 안경은 시력 보조의 기본적인 용도 외에도 증강 또는 가상 현실 기능을 제공하는 착용형 장치로써 다양하게 연구 또는 활용되고 있다. 하지만 안경에 대한 이러한 접근은 안경의 시력과 관련된 기능만을 제공하는 것으로, 안경을 입력 장치로 사용하거나, 안경 본연의 기구학적 구조를 활용하는 노력이 결여되어 있다. 안경의 전면부와 다리를 연결하는 힌지는 지렛대의 원리에 의해 힘의 집중이 발생하는 곳이다. 안경을 착용하였을 때 힌지에 가해지는 예압 패턴의 변화로부터 측두근을 비롯한 안면 근육의 미세한 움직임을 감지할 수 있다. 그 결과, 해부학적으로 측두근 및 눈둘레근의 수축과 이완을 야기하는 저작 및 윙크 활동을 힌지에서 증폭된 힘의 형태로 감지하는 것이 가능하다.

본 연구는 안경 본연의 힌지 구조를 활용하여 측두근의 활동을 객관적이고 자동적으로 감지하는 새롭고 효과적인 방법을 제시한다. 3D 프린팅 된 안경 틀의 좌우 힌지에 로드셀 통합형 무선 모듈을 내장하여 사람마다 다양한 형태 인자에 무관하게 안정적으로 반응하는 시스템을 개발하였다. 이를 통해 기존 연구들이 피부 부착형, 근접형, 또는 소리 감지형 센서를 사용함으로써 얻는 형태적, 운동적, 환경적 제약을 효과적으로 해결하였다. 본 연구에서는 10명의 사용자 학습을 통해 앉아서 쉬기, 씹기, 걷기, 걸으며 씹기, 말하기, 윙크로 정의된 활동의 신호들을 수집하였다. 수집된 신호는 시간과 주파수 차원의 통계적

특징들로 구성된 84차원의 특징 벡터를 정의하였고, 서포트 벡터 머신 알고리즘과 특징 선택 알고리즘을 통해 씹기, 윙크, 신체 활동을 93.7%의 F_1 점수로 분류하였다.

본 연구는 비방해적이고, 비간섭적인 방법을 통해 섭식 활동 관찰에 대한 새롭고 효과적인 접근을 제시한다. 음식 섭취 활동을 걷기, 말하기, 윙크 등의 다른 활동과 높은 정확도로 구분함으로써, 궁극적으로 음식 섭취 감지 연구가 일상 생활에 실용적으로 적용될 수 있는 발판을 마련하였다. 나아가 안면 근육의 복합적 패턴을 분석하여 표정과 감정을 감지하거나, 수면 중 이갈이나 턱관절 장애 등의 의료적 관찰의 용도로도 활용될 수 있을 것이다.

주요어: 안경, 지렛대 원리, 착용형 장치, 섭식 활동의 관찰, 패턴 인식, 서포트 벡터 머신
학　번: 2011-20752